Journal of Medicinal Chemistry

Article

Discovery of Novel 1-Cyclopentenyl-3-phenylureas as Selective, Brain Penetrant and Orally Bioavailable CXCR2 Antagonists

Hongfu Lu, Ting Yang, Zhongmiao Xu, Xichen Lin, Qian Ding, Yueting Zhang, Xin Cai, Kelly Dong, Sophie Gong, Wei Zhang, Metul Patel, Royston C. B. Copley, Jianing Xiang, Xiaoming Guan, Paul Wren, and Feng Ren

J. Med. Chem., **Just Accepted Manuscript** • DOI: 10.1021/acs.jmedchem.7b01854 • Publication Date (Web): 06 Feb 2018

ACS Publications

Journal of Medicinal Chemistry is published by the American Chemical Society. 1155 Sixteenth Street N.W., Washington, DC 20036

Discovery of Novel 1-Cyclopentenyl-3-phenylureas as Selective, Brain Penetrant and Orally Bioavailable CXCR2 Antagonists

Hongfu Lu,[†] Ting Yang,[†] Zhongmiao Xu,[†] Xichen Lin,[†] Qian Ding,[†] Yueting Zhang,[§] Xin Cai,[‡] Kelly Dong,[‡] Sophie Gong,[‡] Wei Zhang,[‡] Metul Patel,[#] Royston C. B. Copley,[⊥] Jianing Xiang,[†] Xiaoming Guan,[†] Paul Wren,[∥] Feng Ren[,†]*

[†]Neurosciences Therapeutic Area Unit, GSK Pharmaceuticals R&D, 898 Halei Road, Zhangjiang Hi-Tech Park, Pudong, Shanghai 201203, PR China.

[§]R&D Projects Clinical Platforms and Sciences, GSK Pharmaceuticals R&D, 898 Halei Road, Zhangjiang Hi-Tech Park, Pudong, Shanghai 201203, PR China.

[‡]Platform Technology Sciences, GSK Pharmaceuticals R&D, 898 Halei Road, Zhangjiang Hi-Tech Park, Pudong, Shanghai 201203, PR China.

[#]Platform Technology Sciences, GSK Pharmaceuticals R&D, Stevenage, Herts, SG1 2NY, UK.

[‡]Platform Technology & Science, GSK Medicines Research Centre, Gunnels Wood Road, Stevenage, Hertfordshire, SG1 2NY, UK.

[∥]Neurosciences Therapeutic Area Unit, GSK Pharmaceuticals R&D, 1250 S. Collegeville Road,

Collegeville, PA 19426, US.

ABSTRACT. CXCR2 has emerged as a therapeutic target for not only peripheral inflammatory diseases but also neurological abnormalities in the central nervous system (CNS). Herein, we describe the discovery of a novel 1-cyclopentenyl-3-phenylurea series as potent and CNS penetrant CXCR2 antagonists. Extensive SAR studies, wherein molecules' property forecast index (PFI) was carefully optimized for overall balanced developability profiles, led to the discovery of the advanced lead compound **68** with a desirable PFI. Compound **68** demonstrated good *in vitro* pharmacology with excellent selectivity over CXCR1 and other chemokine receptors. Rat and dog pharmacokinetics (PK) revealed good oral bioavailability, high oral exposure, and desirable elimination half-life of the compound in both species. In addition, the compound demonstrated dose-dependent efficacy in the *in vivo* pharmacology neutrophil infiltration "air pouch" model in rodents after oral administration. Further, compound **68** is a CNS penetrant molecule with high unbound fraction in brain tissue.

KEYWORDS. CXCR2 antagonist, 1-cyclopentenyl-3-phenylurea, P-gp, BCRP, CNS penetration, PFI, air pouch

INTRODUCTION

CXCR2, a CXC chemokine receptor of the G-protein-coupled receptor (GPCR) family, is a seven-transmembrane protein with a 67–70 kD molecular weight expressed on neutrophils, granulocytes, NK cells, T lymphocytes, mast cells, monocytes, endothelial cells, megakarocytes, neurons, and oligodendrocytes.[1] CXCR2 and its main cognate ligands CXCL1 (Gro-α) and CXCL8 (IL-8) have been extensively reported as critical pro-inflammatory components of

neutrophil activation and chemotaxis, megakaryocytic proliferation, and angiogenesis.[2-4] Increasing evidence has emerged to implicate the important role of CXCR2 in numerous inflammatory disorders[5] including chronic obstructive pulmonary disease (COPD)[6], rheumatoid arthritis (RA)[7], and atherosclerosis[4]. Recently, CXCR2 inhibitor was reported to reduce metastases and augment anti-PD1 immunotherapy in KPC mice to result in prolonged survival.[8] Likewise, CXCR2 antagonist significantly enhanced the efficacy of immune checkpoint blockage (ICB) treatment in a mouse prostate cancer model.[9] These preclinical data have raised significant interest of CXCR2 as a therapeutic target for cancer immunotherapy. The correlation between CXCR2 expression and human glioma was reported, and CXCR2 inhibition was found to mitigate glioma cell migration.[10] In addition to peripheral immune system, CXCR2 also plays a role in regulating neuronal activity and brain development even though its expression level is low in both human and rodent brains. [11] Increasingly, CXCR2 has been recognized as a potential target for the treatment of CNS diseases such as multiple sclerosis[12] and Alzheimer's disease (AD)[13], and others.[14] Thus, discovery of small molecule CXCR2 antagonists with brain penetration properties may open new opportunities to explore and tackle abnormalities in the CXCL1 (Gro-α)/CXCL8 (IL-8) signaling pathway in CNS diseases.

The first small molecule CXCR2 antagonists were reported in 1998,[15] and since then a number of chemical series of small molecule CXCR2 antagonists with diverse pharmacophores have been developed (Figure 1). Among them, quite a few compounds have been progressed into clinical trials for the treatment of neutrophil-induced pulmonary diseases. Reparixin (**1**), an allosteric inhibitor of CXCR1 with several hundred-fold selectivity over CXCR2, was reported to block CXCL8- and CXCL-1 mediated neutrophil (PMN) migration and was advanced into clinical trials via intravenous administration for delayed graft function and transplant rejection.[16]

Later the compound was re-positioned for a clinical trial for breast cancer. A pyrimidine-based compound, AZD5069 (**2**), with reasonable oral bioavailability was progressed to clinical stage for COPD and asthma and afterwards, a clinic study for cancer treatment was initiated. Compound **2** proved to be a potent CXCR2 antagonist with around 100-fold selectivity over CXCR1.[17] Later, a bicyclic pyrimidine series was reported as dual CXCR2/CCR2 antagonists and a representative, AZ10397767 (**3**), demonstrated nanomolar antagonism activity for both CXCR2 and CCR2.[17,18] Navarixin (**4**, also known as SCH527123 or MK-7123), bearing a novel squaramide core structure, was described as a potent and selective antagonist of CXCR2 with 80-fold selectivity over CXCR1.[19] A phase 2 clinical trial of compound **4** in COPD patients demonstrated clinical benefit of the anti-inflammatory mechanism resulting from CXCR2 antagonism.[20,21] Several other novel chemical series were also disclosed as CXCR2 antagonists including the 5-carbonitrile pyrimidines,[22] 2-amino-quinoxalines,[23] and boronic acid derivatives containing aminopyridines/aminopyrimidines.[24] However, none of these structures was able to be progressed to clinic testing. Among all the small molecule CXCR2 antagonists reported to date, the diarylurea series was the first disclosed[15] and the successful chemical series from which a couple of compounds had been advanced to the clinic. SB-332235 (**5**), even though not progressed to the clinic, was an important diarylurea early tool compound for mechanistic explorations of CXCR2 antagonism for COPD and AD.[25] The first diarylurea-based CXCR2 antagonist advanced to clinical trial is SB-656933 (**6**), which has been tested in COPD and cystic fibrosis (CF) patients.[26] Further development of compound **6** was discontinued due to lack of significant lung function improvement in clinics during the dosing regimen[26b] and in favor of a more attractive diarylurea analogue, Danirixin (**7**, also known as GSK1325756).[27] Currently compound **7** is in phase II clinical trial for COPD. Extensive literature reports have been focused

on the small molecule CXCR2 antagonists for the treatment of peripheral indications.[28] On the other hand, however, little has been disclosed on brain penetration characteristics of compounds. Most recently, a CNS penetrant CXCR2 antagonist based on the diarylurea skeleton (**8**) was disclosed, and the compound promoted remyelination in mouse brain in the cuprizone-induced demyelination model.[29] The series including compound **8** was reported to have low unbound fractions in plasma[29] which might be attributed to its high lipophilicity (cLogP) and high property forecast index (PFI). PFI, the sum of hydrophobicity value and number of aromatic rings, has evolved as one of the key "drug-likeness" measurements as supported by its correlations with compound developability properties including solubility, membrane permeability, plasma protein binding, cytochrome P450 inhibition, hERG binding, and promiscuity, etc.[30]

Herein, we report the discovery of a novel 1-cyclopentenyl-3-phenylurea series as brain penetrant and selective CXCR2 antagonists for the potential treatment of CNS diseases. In our work, replacing one aromatic ring of the previously reported diarylureas with the aliphatic cyclopentenyl group provides marked reduction of PFI thus significant improvement of the developability profile (plasma protein binding, solubility, etc.) of the series.

RESULTS AND DISCUSSION

Structure-Activity Relationships and CNS Penetration. We started our exploration from the known CNS penetrant diarylurea series where compound **8** was identified as the lead.[29] However, compound **8** might suffer from an active demethylation metabolite issue wherein the methyl group of the *N*-methyl piperidine was observed to be metabolized to a significant extend *in vitro* in human liver microsomes.[31] Therefore, among the diarylurea analogues without the *N*-methyl piperidine substitution, taken into consideration of compounds' potency and "drug-

likeness" properties such as molecular weight (MW) and PFI, compound **9** (Table 1) was selected as the chemistry starting point. Our initial work was focused on replacing the 2-chloro-3-fluorophenyl group (R, Table 1) of **9** with aliphatic rings to reduce PFI. The cyclohexyl analogue (**10**) demonstrated much reduced PFI (6.7) compared to compound **9** (8.2), but decreased CXCR2 antagonism activity (pIC_{50} = 7.3) by ~100 fold in the CXCR2 Tango assay, which determined compounds' functional potency at recombinant CXCR2 receptors. Introduction of methyl (**11**, pIC_{50} = 6.5) or methoxyl (**12**, pIC_{50} = 5.8) substitutions to the cyclohexyl ring resulted in even lower potencies. 6-Membered saturated heterocyclic rings including tetrahydropyran (**13**, **14**) and piperidine (**15**, pIC_{50} < 5.0) were not tolerated, indicating a hydrophobic pocket occupied by the R group. We then explored the ring size and found that the 5-membered cyclopentane ring (**16**) demonstrated higher potency (pIC_{50} = 8.0) and lower PFI (6.0) than its 6-membered analogue (**10**). Efforts to further improve CXCR2 antagonist activity by introducing hydrophobic and/or hydrophilic substitutions (**17**–**21**) failed to provide any compound with higher potency. The *ortho*-substitution (**17**, pIC_{50} = 8.0) demonstrated better potency than the *meta*-substitution (**18**, pIC_{50} = 6.7). Increasing the size of the *ortho*-substitution resulted in decreased potency (**19**, pIC_{50} = 7.2), suggesting that small substitutions be preferred. The hydrophilic substitution was poorly tolerated (**20**, pIC_{50} = 6.6), further supporting the existence of a hydrophobic binding pocket. The di-substitution at the *ortho*-position of the cyclopentanyl group resulted in low activity (**21**, pIC_{50} = 6.8), likely due to the unfavorable steric effect. Sterically less hindered spiro and fused analogues afforded better potencies (**22**, **23**). As expected, the hydrophilic pyrrolidine group led to an inactive compound (**24**, pIC_{50} < 5.0). We then started to explore the unsaturated rings to increase planarity which might better mimic aromatic rings. Intriguingly, the cyclopentenyl ring afforded slightly improved potency (**25**,

pIC$_{50}$ = 8.2) compared with the cyclopentanyl analogue (**16**). A breakthrough was achieved when a methyl substitution was introduced to the α-position of the cyclopentenyl group (**26**, pIC$_{50}$ = 9.4). The Cl substitution provided comparable potency (**27**, pIC$_{50}$ = 9.0) whereas sterically more hindered and less hindered substitutions were less potent (**28**, **29**). Di-substituted cyclopentenyl groups (**30**, **31**) were observed to result in decreased potency. Again, ring size was explored and, similarly, 6-membered unsaturated rings (**32**–**34**) were less potent than their 5-membered counterparts. Thus, the 2-methylcyclopentenyl (**26**) was identified as the best right-hand-side (RHS) R group for future SAR studies.

Compounds in Table 1 were synthesized and tested as racemates. In order to further understand the effect of cyclopentenyl stereochemistry on the CXCR2 antagonism activity, several pairs of the single known *(R)*- and *(S)*-enantiomers were designed and synthesized. It was worth mentioning that the 2-chlorocyclopent-2-enamine was synthetically more accessible in both *(R)*- and *(S)*-configurations comparing to the 2-methylcyclopent-2-enamine, thus the 2-Cl-cyclopentenyl analogues were used for stereochemistry SAR exploration (Table 2). Generally, the *(R)*-isomers (**35**–**37**) were observed to be ~100 fold more potent than the *(S)*-isomers (**35'**–**37'**) as evaluated in the CXCR2 Tango assay. When R was oxetane, the potency difference between the *(R)*-isomer (**38**, pIC$_{50}$ = 6.5) and the *(S)*-isomer (**38'**, pIC$_{50}$ = 5.6) was less significant although still ~10 fold. Having established the SAR that the 2-methylcyclopentene was the best RHS group and the (*R)*-configuration was more favored than the *(S)*-configuration, future SAR studies were focused on analogues containing the *(R)*-2-methylcyclopentenyl ring.

SAR studies were then focused on the left-hand-side (LHS) especially on R^1 and R^2 substitutions (Table 3). The aim was to balance the overall profile of the series including potency, solubility, permeability, and P-glycoprotein (P-gp)/breast cancer resistance protein

(BCRP) efflux which are *in vitro* measurements for CNS penetration property[33]. Exploration of the R^1 substitution started from the *tert*-butyl group (**39**), which demonstrated high CXCR2 antagonist potency (pIC_{50} = 9.0) in the Tango assay. It was further evaluated in the human whole blood (HWB) Gro-α induced CD11b expression assay, which measured the functional potency at the native CXCR2 receptor, and was found quite active (pIC_{50} = 6.5). In addition, compound **39** showed high cell permeability (364 nm/s) and proved not to be a P-gp/BCRP efflux substrate, resulting in good CNS penetration. However, the compound demonstrated very low solubility (1.2 μg/mL) in fasted state simulated intestinal fluids (FaSSIF),[34] likely due to its high PFI (7.4). Incorporating electron withdrawing group (EWG) such as F or CF_3 to the *tert*-butyl group provided analogues (**40**, **41**) with slightly reduced PFI (6.6 and 6.7, respectively) however, not surprisingly, only marginal improvements in FaSSIF solubility were observed. Further reducing PFI by replacing two methyl groups with two F led to compound **42** (PFI = 4.3) with much improved solubility (50.8 μg/mL). Introduction of a dimethylamino group resulted in a significant drop in CXCR2 antagonist potency (**43**, pIC_{50} = 6.9) even though its solubility was high (395.4 μg/mL). Another dimethylamino derivative (**44**) demonstrated improved potency (pIC_{50} = 8.7), however it proved to be a strong P-gp/BCRP substrate (ER = 12.6) thus carried high risk for adequate CNS penetration. Intrigued by the high solubility of **43** and **44**, a series of nitrogen-containing derivatives were synthesized and evaluated (**45**–**51**). Among them, compounds **50** and **51** demonstrated balanced overall profiles for further progression and the rest of compounds were less attractive due to P-gp/BCRP liabilities (**45**, **46**) or low potency (**47**, **49**). Substitutions at the R^2 position were also investigated. The acidity of the phenol group was believed to be critical for the potency of the series, we thus limited our exploration to the EWG only, in order to maintain or increase its acidity. Replacing the Cl of **39** with a stronger electron-

withdrawing CN group provided compound **52** with improved potency (pIC_{50} = 9.7), presumably due to the increased acidity of the phenol. In addition, **52** demonstrated much lower PFI and as a result high solubility (685.6 μg/mL). On the other hand, as the compound got more polar its passive permeability decreased (90 nm/s). A similar profile was also observed with another CN derivative (**53**) with even lower permeability (30 nm/s).

Based on the overall properties especially potencies and P-gp/BCRP profiles, several representative analogues (**40**–**42**, **50**–**52**) were selected for evaluation for *in vivo* CNS penetration using a rat short oral absorption (SOA) model (Table 4). The brain-to-blood ratio (K_p) of the area under curve (AUC) of compound **40** was measured to be 0.16 after oral gavage to rats. Intriguingly, its free unbound fraction in both brain ($F_{u,br}$ = 3.4%) and blood ($F_{u,bl}$ = 1.1%) were measured to be significantly higher than the diarylurea exemplars (e.g. compound **9**)[29] which was likely due to its lower PFI. Increasingly, the brain-to-blood ratio of free unbound drug concentration ($K_{p,uu}$) has been described as a critical parameter for CNS penetration.[35] $K_{p,uu}$ for compound **40** was determined to be 0.48. The trifluoromethyl analogue **41** also demonstrated good CNS penetration in terms of both total drug exposure (K_p = 0.20) and free unbound drug exposure ($K_{p,uu}$ = 0.59). With a slightly higher PFI, its free unbound fractions in both brain ($F_{u,br}$ = 2.1%) and blood ($F_{u,bl}$ = 0.70%) were slightly lower than compound **40**. The nitrogen-containing analogues (**50** and **51**) demonstrated high peripheral drug exposure with dose normalized area under curve (DNAUC) of 2580 and 11721 (ng·h/mL)/(mg/kg), respectively. However, their K_p values were measured very low (0.06 and 0.03, respectively) and as a result their $K_{p,uu}$ could not be determined with meaningful values. Both **50** and **51** were thus considered peripherally restricted compounds. Compound **52** with the CN substitution also demonstrated low CNS penetration as evidenced by its low brain-to-blood ratio of AUC (K_p = 0.03). It was

noteworthy that all the compounds evaluated with low brain penetration showed PFI values < 5 (4.3, 3.7, 3.7 and 4.1 for compound **42**, **50**, **51** and **52**, respectively), whereas compounds with high brain penetration showed PFI values > 5 (6.6 and 6.7 for compound **40** and **41**, respectively). SAR suggested that, for this 1-cyclopentenyl-3-phenylurea series, compounds with PFI > 5 might have better potentials to be brain penetrant. On the other hand, high PFI has been shown to be associated with low solubility, high protein binding, and other developability risks.[30] We thus focused our efforts on the compounds with PFIs between 5 and 7, for the purpose of achieving balanced profiles of CNS penetration and developability (solubility, free unbound fraction, etc.).

Due to low solubility for alkyl/haloalkyl groups and high efflux ratios for *N*-containing groups as R^1 substitutions, *O*-containing substituents were then investigated to balance solubility and efflux ratio (Table 5). Compound **54** with a methoxyl substitution demonstrated balanced profile of FaSSIF solubility (72.0 μg/mL) and P-gp/BCRP efflux ratio (3.2), however its potency, especially when measured in the human whole blood CD11b assay, was not optimal (pIC_{50} = 6.4). Addition of a 4-membered oxetane ring (**55**) provided much improved CXCR2 antagonist potency in the Tango assay whereas the solubility decreased dramatically (7.0 μg/mL). Increasing the ring size (**56**–**58**) failed to improve the potency and/or resulted in low solubility (**58**). The HWB potency was slightly improved (pIC_{50} = 6.7) when the tetrahydropyran was directly connected to the sulfonyl group (**59**) but low solubility was observed. Replacing the methyl group of **59** with an ethyl group (**60**) led to higher solubility but lower HWB potency. Introduction of F atom provided compounds (**61**–**63**) with increased P-gp/BCRP efflux liability. Changing the position of oxygen atom in tetrahydropyran (**64**, **65**) failed to provide compounds with more balanced profile of solubility and P-gp/BCRP efflux. We then switched to a 5-

membered tetrahydrofuran ring with 5 < PFI < 6 (**66**–**68**) and, to our delight, compound **68** demonstrated a balanced profile of solubility (21.0 μg/mL) and P-gp/BCRP efflux ratio (2.0). In addition, the HWB potency of **68** (pIC_{50} = 7.4) proved to be the highest amongst all the compounds explored. Introduction of a F atom (**69**) resulted in an increased efflux ratio, similar to the 6-membered tetrahydropyran analogues. The hydroxyl (**70**) and spiro (**71**) substitutions led to high efflux ratios (26.8 and 25.5, respectively), likely due to their low PFIs (< 5).

Based on their overall profiles including potency, solubility, and P-gp/BCRP efflux, compounds **56**, **67**, and **68** were selected for rat SOA studies for *in vivo* CNS penetration evaluation (Table 6). Among them, compound **68** demonstrated the highest $K_{p,uu}$ (0.63), indicating a good *in vivo* brain penetration property. It showed a higher brain penetration property comparing to the previously reported CNS penetrant compound (**8**)[29], the $K_{p,uu}$ of which was determined to be 0.18. In addition, the unbound fractions of compound **68** were measured to be reasonable in both rat blood ($F_{u,bl}$ = 2.7%) and human plasma ($F_{u,pl}$ = 1.9%), which were more than 10-fold higher than the unbound fraction of compound **8** in human plasma ($F_{u,pl}$ = 0.13%) described previously.[29] The balanced profile of CNS penetration and free unbound fraction of compound **68** was likely due to its desirable PFI (5.8), supporting the belief that ideal values of PFIs of the series are between 5 and 7 as discussed previously. It was noteworthy that the free unbound fraction of **68** in brain ($F_{u,br}$ = 12.3%) was observed to be much higher than in blood. This phenomenon was consistent throughout the series and likely due to the acidic character of the sulfone substituted phenol group unique within this 1-cyclopentenyl-3-phenylurea series. The diastereoisomer of **68**, compound **67**, had the same PFI (5.8) thus its free unbound fractions in both blood ($F_{u,bl}$ = 3.6%) and brain ($F_{u,br}$ = 10.6%) were similar to **68**. However, the CNS penetration properties of **67** measured as both K_p (0.08) and $K_{p,uu}$ (0.23) were less attractive.

Compound **56** demonstrated a good CNS penetration profile whereas its low exposure in blood [63.8 (ng·h/mL)/(mg/kg)] was a concern and prohibited further progression.

DMPK. Lead compounds **40** and **68** were further progressed in an *in vivo* PK study in rats following 1 mg/kg intravenous (IV) and 2 mg/kg oral administration (Table 7). Both compounds showed low clearance and high exposure in rat, consistent with their profile from the *in vivo* rat SOA study. The half-life ($T_{1/2}$) of compound **68** (4.3 h) was longer than that of compound **40** (2.5 h), likely due to its lower clearance (9.1 mL/min/kg) compared to **40** (15.7 mL/min/kg). The DNAUC values for compounds **40** and **68** were determined to be 1071 and 1829 (ng·h/mL)/(mg/kg), respectively. The oral exposure of both compounds was measured high with DNAUC values of 961 (ng·h/mL)/(mg/kg) for **40** and 860 (ng·h/mL)/(mg/kg) for **68**, corresponding to 88% and 47% oral bioavailability, respectively. Compound **68** was selected as the advanced lead compound due to its longer $T_{1/2}$, better solubility, and higher free unbound fraction compared to compound **40**. An *in vivo* dog PK study was conducted for compound **68** and low clearance (5.6 mL/min/kg), reasonable $T_{1/2}$ (3.6 h), high oral exposure [2298 (ng·h/mL)/(mg/kg)], and good oral bioavailability (76%) were observed, which were consistent with the rat profile. In addition, the *in vitro* metabolic stability of compound **68** in human, rat, and dog hepatocytes was determined (Table 8). The result revealed that the compound was most stable in human hepatocytes [Cl_{int} = 0.79 (mL/min/g)] and least stable in rat hepatocytes [Cl_{int} = 7.7 (mL/min/g)].

In Vitro Pharmacology in Mouse and Human Whole Blood. The ability of compound **68** to inhibit CXCR2 receptor activation was assessed in whole blood Gro-α induced CD11b expression assays and quantified by flow cytometry. In the mouse whole blood assay (Figure 2a), compound **68** inhibited Gro-α induced CD11b expression with a IC_{50} value of 5.9 nM (N = 3),

comparable to the control compound Navarixin[19,20] (IC_{50} = 8.1 nM). It was worth mentioning that the maximal response of compound **68** was less than that of Navarixin, around two thirds of CD11b inhibition driven by Navarixin at 10 μM, suggesting a partial inhibitory effect of compound **68** in mouse whole blood. In contrast, in human whole blood CD11b assay (Figure 2b) compound **68** (similar to Navarixin) fully inhibited Gro-α induced CD11b expression with an IC_{50} value of 0.04 μM (N = 5) which was 17-fold more potent than that of Navarixin (IC_{50} = 0.68 μM). In addition, compound **68** was 12-fold more potent than the reported CNS penetrant compound **8**[29] (IC_{50} = 0.50 μM) in this HWB assay.

In Vitro Chemokine Selectivity. Compound **68** demonstrated excellent selectivity for CXCR2 antagonist activity over other CXC and CC chemokine receptors (Table 9). A total of 18 CXC and CC chemokine receptors including CXCR2 were evaluated in both agonism and antagonism modes in β-arrestin assays and, among them, compound **68** was measured to be inactive (IC_{50}s > 10 μM) in all assays except for CXCR2 and CXCR1. IC_{50}s of the compound on CXCR2 and CXCR1 were 5.2 nM and 3.8 μM, respectively. Thus, compound **68** was determined to be a highly selective CXCR2 antagonist with ~730-fold selectivity over CXCR1 and >1900-fold selectivity over all other chemokine receptors evaluated.

In Vivo Pharmacology in Mouse and Rat. The effects of compound **68** on peripheral inflammatory cell infiltration induced by 2% carrageenan was tested using mouse and rat air pouch models.[36] As shown in Figure 3a, compound **68** significantly inhibited neutrophil infiltration into mouse air pouch, as compared to vehicle (One way ANOVA), 4 h after carrageenan induction at 1, 3, 10 mg/kg oral dosing twice daily (BID). Similar *in vivo* pharmacology was observed in the rat air pouch model (Figure 3b). In this species, compound **68**

demonstrated a marked dose-dependent inhibition of neutrophil migration from 1 mg/kg to 3 mg/kg to 10 mg/kg BID oral dosing.

Synthetic Chemistry. Convergent synthetic routes for the syntheses of 1-cyclopentenyl-3-phenylureas were developed as illustrated in the syntheses of key compounds **40** and **68**. Both compounds were assembled from the common RHS chiral amine intermediate (**75**) and the corresponding LHS aminophenol intermediates (**82** for compound **40** and **85** for compound **68**), as shown in Scheme 1. Synthesis of chiral amine **75** was initiated from the commercial starting material, ketone **72**. Enantioselective reduction of the ketone group of **72** catalyzed by (*R*)-CBS[37] provided alcohol **73** in quantitative yield, and the enantiomeric excess (*ee*) was determined in the next step. Stereospecific reversion of the chiral alcohol with phthalimide by Mitsunobu reaction afforded chiral phthalimide intermediate **74** with 74% *ee* favoring the (*R*)-isomer. Chiral purification of the mixture by supercritical fluid chromatography (SFC) afforded enantiomerically pure intermediate **74** as the (*R*)-isomer with >98% *ee*. Treatment of **74** with hydrazine at elevated temperature provided the common RHS intermediate, the chiral amine **75**.

Synthesis of the lead compound **40** was initiated from the reported starting material, thiol **76** (Scheme 2).[32] **76** was treated with ethyl 2-bromo-2-methylpropanoate to afford the thiol ether **77**, which was then oxidized by *m*-CPBA to afford sulfone **78** in 64% yield over two steps. Reduction of the ethyl ester of **78** with DIBAL-H provided the alcohol **79**. The hydroxyl group of **79** was converted to trifluoromethanesulfonate (**80**) and, after treatment with TBAF, the F-containing intermediate **81** was obtained in good yield (46% over three steps). Hydrolysis of the benzoxazole moiety in strong acidic condition at elevated temperature gave the LHS intermediate, aminophenol **82**. Coupling of LHS **82** with the transient isocyanate intermediate derived from RHS **75** provided the final compound **40** in good isolated yield (58%).

For the synthesis of lead compound **68** (Scheme 3), the starting material **83** was prepared in large quantities following a published procedure.[28] Compound **83** was treated with methyl iodide in the presence of LHMDS to afford the intermediate **84** as an enantiomeric mixture at the tetrahydrofuran moiety. The benzoxazole group of **84** was hydrolyzed under acidic condition to afford the LHS aminophenol **85** in good isolated yield over two steps (66%). Similarly, the LHS **85** was coupled with the isocyanate derived from RHS **75** to produce the diastereomeric mixture **66** in high yield (96%). The two diastereomers of **66** were separated by SFC to afford the desired single diastereomer **68** in 22% isolated yield (>93% *de*). The absolute stereochemistry of the 3-methyltetrahydrofuran-3-yl group of compound **68** was established unambiguously as the (*S*)-isomer from crystal structure.

X-ray Crystallography. The absolute configuration of compound **68** was determined using single crystal X-ray diffraction techniques. The compound crystallizes with two independent molecules in the asymmetric unit. One of these is shown in Figure 4. For both molecules, the 3-methyltetrahydrofuran-3-yl groups are found to be disordered over two positions but the (*S*)-configuration for this moiety is maintained within the model throughout (see Supporting Information for further information). The chiral center of the 2-methylcyclopent-2-enamine moiety was confirmed to be (*R*), consistent with the reported stereochemistry assignment generated from (*R*)-CBS reduction. Intermolecular hydrogen bonds between urea groups alternately link the two independent molecules into chains within the structure. An intramolecular interaction exists in both molecules between the hydroxyl group and a sulfonyl oxygen atom.

CONCLUSIONS

In summary, a series of novel 1-cyclopentenyl-3-phenylureas were discovered as potent, brain penetrant, and orally available CXCR2 antagonists. Extensive SAR studies to improve solubility, protein binding, and *in vitro* and *in vivo* CNS penetration properties by carefully optimizing molecules' PFI led to the discovery of the advanced lead compound **68**. Compound **68** demonstrated desirable PFI (5.8), good solubility (21.0 μg/mL), and high free unbound fraction in both blood ($F_{u,bl}$ = 2.7%) and brain ($F_{u,br}$ = 12.3%). Rat and dog PK studies revealed moderate to good oral bioavailability (47% and 76%, respectively) with high oral exposure [DNAUC: 860 and 2298 (ng·h/mL)/(mg/kg), respectively] and desirable $T_{1/2}$ (4.3 and 3.6 h, respectively) in both species. Compound **68** inhibited human whole blood Gro-α induced CD11b expression with a IC_{50} value of 0.04 μM, 17-fold more potent than a reported clinical compound Navarixin (IC_{50} = 0.68 μM). Screening of **68** on a panel of 18 chemokine receptors highlighted potent inhibition of CXCR2 (IC_{50} = 5.2 nM) with ~730-fold selectivity over CXCR1 and >1900-fold selectivity over all other chemokine receptors tested (IC_{50}s >10 μM). Compound **68** dose-dependently reduced neutrophil infiltration *in vivo* in rat and mouse "air pouch" models upon oral administration (1, 3, and 10 mg/kg BID). In addition, good CNS penetration profile of compound **68** was observed in rat *in vivo* SOA study ($K_{p,uu}$ = 0.63). Compared to the reported CNS penetrant compound **8**, compound **68** demonstrated much better potency (12 fold) in human whole blood assay, significantly higher unbound fraction in human plasma (>10 fold), and improved brain penetration as measured by $K_{p,uu}$ (>3 fold). The compound might represent a promising candidate for not only peripheral inflammatory diseases but also a range of CNS indications.

EXPERIMENTAL SECTION

Chemistry. The syntheses of the compounds **40**, **66** and **68** are described below. Detailed experimental procedures for the syntheses of all other compounds, their intermediates, and

characterization data are provided in the Supporting Information. Liquid chromatography mass spectrometry (LCMS) was used to determine the purity of compounds, and all tested compounds were determined with ≥ 95% purity.

Materials and Methods. Reagents were purchased from commercial suppliers and used directly without further purification. ^{1}H NMR and ^{13}C NMR spectra were measured on Bruker 400/600 NMR spectrometer wherein $CDCl_3$ (deuterochloroform), CD_3OD (deuterated methanol), or DMSO-d_6 (hexadeuterio-dimethyl sulfoxide) were used as the solvents and TMS (tetramethylsilane) was used as the internal standard. Chemical shifts (δ) were given in parts per million (ppm) downfield from the internal standard TMS signal. In NMR spectra, the following abbreviations were used for multiplicity: s = singlet, d = doublet, t = triplet, q = quartet, m = multiplet, dd = doublet of doublets, dt = doublet of triplets, ddd = doublet of doublet of doublets, br = broad. *J* was used to indicate the NMR coupling constant measured in Hertz. High resolution mass (HRMS) measurement was achieved using an orthogonal acceleration time-of-flight (oa-TOF) SYNAPT G2 HDMS^{TM} equipped with a positive mode of electrospray ionization (ESI) (Waters, Manchester, UK). LCMS analysis was conducted on Agilent 1200SL-6110 under the acidic condition, water containing 0.05 % TFA/acetonitrile as the mobile phase on Agilent SB-C18 column (1.8 μm, 4.6 x 30 mm), with MS and photodiode array detector (PDA). The following conditions were used for LCMS: a gradient from 5 to 95% in 5 min (or 6 min) and held at 95% for 1 min; UV detection at 214 and 254 nm; a flow rate of 1.5 ml/min; full scan; mass range from 100 to 1000 amu. Column chromatography purifications were performed on Isco or Biotage with a detector with UV wavelength at 254 nm and 280 nm, using a pre-packed silica gel column.

The preparation of the target compounds 40, 66 and 68.

Synthesis of (*R*)-1-(4-chloro-3-((1-fluoro-2-methylpropan-2-yl)sulfonyl)-2-hydroxyphenyl)-3-(2-methylcyclopent-2-en-1-yl)urea (40). To a solution of (*R*)-2-methylcyclopent-2-enamine, hydrochloride salt (**75**, 560 mg) in toluene (36 mL) was added triphosgene (746 mg). The reaction mixture was refluxed for 6 hours, and then cooled to room temperature to give the fresh prepared isocyanate solution. To a solution of 6-amino-3-chloro-2-((1-fluoro-2-methylpropan-2-yl)sulfonyl)phenol (**82**, 100 mg) in pyridine (5 mL) was added the above isocyanate solution in toluene (4 mL). The reaction mixture was stirred at room temperature for overnight. The reaction mixture was concentrated and the resulting residue was purified by prep-HPLC to give (*R*)-1-(4-chloro-3-((1-fluoro-2-methylpropan-2-yl)sulfonyl)-2-hydroxyphenyl)-3-(2-methylcyclopent-2-en-1-yl)urea (**40**, 70 mg, 58% yield) as a white solid. ^{1}H NMR (400 MHz, DMSO-d_6) δ 10.31 (s, 1H), 8.38 (d, J = 8.8 Hz, 1H), 8.16 (s, 1H), 7.12 (d, J = 8.8 Hz, 1H), 7.07 (d, J = 8.3 Hz, 1H), 5.51 (br. s., 1H), 4.73 (s, 1H), 4.62 (s, 1H), 4.45–4.57 (m, 1H), 2.10–2.37 (m, 3H), 1.66 (s, 3H), 1.45–1.57 (m, 1H), 1.35–1.42 (m, 6H); ^{13}C NMR (151 MHz, DMSO-d_6) δ 155.1, 148.1, 140.6, 130.8, 127.4, 124.1, 124.0, 123.9, 116.6, 85.2, 84.0, 67.8, 58.0, 32.6, 30.0, 17.5, 14.3. LCMS(ESI) *m/z* 405 $[M+H]^+$. HRMS (EI) *m/z*: $[M+H]^+$ calcd for $C_{17}H_{23}ClFN_2O_4S$ 405.1051, found 405.1045.

Synthesis of 1-(4-chloro-2-hydroxy-3-((3-methyltetrahydrofuran-3-yl)sulfonyl)phenyl)-3-((*R*)-2-methylcyclopent-2-en-1-yl)urea (66). To a solution of 6-amino-3-chloro-2-((3-methyltetrahydrofuran-3-yl)sulfonyl)phenol (**85**, 3.0 g) in pyridine (20 mL) was added the fresh prepared isocyanate solution (as described in the synthesis of **40**). The mixture was stirred at 40 °C for 12 h. Ice-water (30 mL) was added to the above solution and the mixture was extracted with DCM (2×100 mL). The combined organic layers were dried over sodium sulphate, filtered and concentrated *in vacuo*. The resulting residue was purified by silica gel column

chromatography eluting with 0–80% ethyl acetate in petroleum ether to give 1-(4-chloro-2-hydroxy-3-((3-methyltetrahydrofuran-3-yl)sulfonyl)phenyl)-3-((*R*)-2-methylcyclopent-2-en-1-yl)urea (**66**, 4.1 g, 96% yield) as a white solid. ^{1}H NMR (400 MHz, DMSO-d_6) δ 10.51 (s, 1H), 8.37 (d, J = 9.0 Hz, 1H), 8.20 (s, 1H), 7.15 (d, J = 8.8 Hz, 1H), 7.08 (d, J = 8.6 Hz, 1H), 5.51 (s, 1H), 4.47–4.58 (m, 1H), 4.33 (d, J = 10.0 Hz, 1H), 3.75–3.89 (m, 2H), 3.60 (d, J = 10.0 Hz, 1H), 2.67 (dt, J = 13.3, 7.9 Hz, 1H), 2.09–2.37 (m, 3H), 1.90–2.02 (m, 1H), 1.66 (s, 3H), 1.44–1.60 (m, 4H); ^{13}C NMR (101 MHz, DMSO-d_6) δ 155.1, 148.0, 140.6, 131.0, 127.4, 124.1, 123.5, 117.1, 73.7, 73.3, 67.8, 58.0, 34.3, 32.6, 30.0, 20.3, 14.3. LCMS(ESI) *m/z* 415 $[M+H]^+$. HRMS (EI) *m/z*: $[M+H]^+$ calcd for $C_{18}H_{24}ClN_2O_5S$ 415.1094, found 415.1085.

Synthesis of 1-(4-chloro-2-hydroxy-3-(((*S*)-3-methyltetrahydrofuran-3-yl)sulfonyl)phenyl)-3-((*R*)-2-methylcyclopent-2-en-1-yl)urea (68). The compound 1-(4-chloro-2-hydroxy-3-((3-methyltetrahydrofuran-3-yl)sulfonyl)phenyl)-3-((*R*)-2-methylcyclopent-2-en-1-yl)urea (**66**, 3.0 g) was separated by supercritical fluid chromatograpy (SFC) and purified by mass detected auto purification system (MDAP) under acidic condition to afford 1-(4-chloro-2-hydroxy-3-(((*S*)-3-methyltetrahydrofuran-3-yl)sulfonyl)phenyl)-3-((*R*)-2-methylcyclopent-2-en-1-yl)urea (**68**, 666 mg, 22% yield) as a white solid. HPLC: Chiralpak IC column (4.6*250 mm, 5 uM), 1:1 ACN/IPA (containing 0.5% DEA), CO_2 flow rate: 2.55 mL/min; co-solvent flow rate: 0.45 mL/min; back pressure: 120 bar); t_r = 16.9 min; >93% *de*; ^{1}H NMR (400 MHz, DMSO-d_6) δ 10.53 (s, 1H), 8.36 (d, J = 8.8 Hz, 1H), 8.17 (s, 1H), 7.14 (d, J = 8.8 Hz, 1H), 7.05 (d, J = 8.3 Hz, 1H), 5.51 (s, 1H), 4.49–4.63 (m, 1H), 4.33 (d, J = 10.3 Hz, 1H), 3.76–3.89 (m, 2H), 3.61 (d, J = 10.0 Hz, 1H), 2.68 (dt, J = 13.3, 7.9 Hz, 1H), 2.10–2.35 (m, 3H), 1.91–2.02 (m, 1H), 1.67 (s, 3H), 1.44–1.58 (m, 4H); ^{13}C NMR (151 MHz, DMSO-d_6) δ 155.1, 148.0, 140.6, 131.0, 127.4, 124.1, 124.1, 123.5, 117.1, 73.7, 73.3, 67.8, 58.1, 34.4, 32.6, 30.0, 20.3, 14.3.

LCMS(ESI) *m/z* 415 $[M+H]^+$; HRMS (EI) *m/z*: $[M+H]^+$ calcd for $C_{18}H_{24}ClN_2O_5S$ 415.1094, found 415.1097.

The preparation of the intermediates 73–75, 77–82, 84–85.

Synthesis of (*S*)-2-methylcyclopent-2-enol (73). To a solution of (*R*)-CBS catalyst (1 M in toluene, 31.8 mL) in anhydrous THF (20 mL) at –60 °C was added 2-methylcyclopent-2-enone (**72**, 15.3 g) and BH_3·THF (1 M in THF, 111 mL). The mixture was stirred at this temperature for 1 h. Methanol (150 ml) was added to the reaction and the resulting mixture was diluted with brine (150 mL). The aqueous layer was extracted with DCM (2×200 mL). The combined organic layers were dried over Na_2SO_4, filtered and concentrated *in vacuo* to give (*S*)-2-methylcyclopent-2-enol (**73**, 16.0 g) as a yellow oil. ^{1}H NMR (400 MHz, $CDCl_3$) δ 5.45 (s, 1H), 4.51 (s, 1H), 2.42–1.98 (m, 4H), 1.70 (s, 3H).

Synthesis of (*R*)-2-(2-methylcyclopent-2-en-1-yl)isoindoline-1,3-dione (74). To a solution of (*S*)-2-methylcyclopent-2-enol (**73**, 16.0 g) and phthalimide (36.0 g) in THF (240 mL) was added PPh_3 (77.0 g) under nitrogen, followed by the addition of DIAD (63.4 mL) at 0 °C. The reaction mixture was stirred at 0 °C for overnight. The solvent was removed *in vacuo* and the resulting residue was directly purified by column chromatography eluting with petroleum ether/ethyl acetate (10:1) to give a crude product (74% *ee*), which was further purified by supercritical fluid chromatography (SFC) to afford (*R*)-2-(2-methylcyclopent-2-en-1-yl)isoindoline-1,3-dione (**74**, 10.6 g, 28% yield over two steps, >98% *ee*) as a white solid. Chiral HPLC (Column: AD-H, 4.6*250 mm, 5 μm, MeOH/CO_2 = 10%, column temperature: 40 °C, CO_2 flow rate: 2.7 mL/min): t_R = 2.17 min, >98% *ee*; ^{1}H NMR (400 MHz, $CDCl_3$) δ 7.83 (dd, *J* = 5.4, 3.1 Hz, 2H), 7.76–7.61 (m, 2H), 5.68 (s, 1H), 5.21 (d, *J* = 7.4 Hz, 1H), 2.69 (dd, *J* = 5.7, 3.5 Hz, 1H), 2.42–2.30 (m, 2H), 2.22–2.12 (m, 1H), 1.61 (s, 3H); LCMS(ESI) *m/z* 228 $[M+H]^+$.

Synthesis of (*R*)-2-methylcyclopent-2-enamine (75). To a solution of (*R*)-2-(2-methylcyclopent-2-en-1-yl)isoindoline-1,3-dione (**74**, 10.7 g) in ethanol (150 mL) was added hydrazine (85% in water, 3.0 mL). After refluxing for 3 hours, the reaction mixture was cooled to room temperature. The precipitate was filtered and the filter cake was rinsed with EtOH (10 mL). To the filtrate was added HCl in dioxane (4 M, 5 mL) and the mixture was concentrated. The resulting residue was dissolved in water, and then freeze dried to afford (*R*)-2-methylcyclopent-2-enamine hydrochloride salt (**75**, 6.3 g, 100% yield) as a brown solid, which was used in the next step without purification. ^{1}H NMR (400 MHz, DMSO-d_6) δ 8.27 (3 H, br. s.), 5.68 (1 H, s), 3.87–4.02 (1 H, m), 2.32–2.48 (1 H, m), 2.15–2.30 (2 H, m), 1.71–1.85 (1 H, m), 1.78 (3 H, s).

Synthesis of ethyl 2-((2-(tert-butyl)-6-chlorobenzo[d]oxazol-7-yl)thio)-2-methylpropanoate (77). To a solution of 2-(tert-butyl)-6-chlorobenzo[d]oxazole-7-thiol (**76**, 11.0 g) in DMF (80 mL) at room temperature was added ethyl 2-bromo-2-methylpropanoate (9.0 g) and K_2CO_3 (2.9 g). After stirring at 60 °C for 3 h, the reaction mixture was diluted with ethyl acetate (200 mL) and washed by brine (3×150 mL). The organic layer was dried over sodium sulfate, filtered and concentrated *in vacuo* to afford ethyl 2-((2-(tert-butyl)-6-chlorobenzo[d]oxazol-7-yl)thio)-2-methylpropanoate (**77**, 14.8 g) as a white solid. LCMS(ESI) *m/z* 356 $[M+H]^+$.

Synthesis of ethyl 2-((2-(tert-butyl)-6-chlorobenzo[d]oxazol-7-yl)sulfonyl)-2-methylpropanoate (78). To a solution of ethyl 2-((2-(tert-butyl)-6-chlorobenzo[d]oxazol-7-yl)thio)-2-methylpropanoate (**77**, 14.8 g) in dichloromethane (200 mL) at room temperature was added *m*-CPBA (20.6 g). The mixture was stirred at room temperature overnight. The reaction mixture was added saturated aqueous Na_2SO_3 solution and was washed with saturated sodium

carbonate solution (100 mL) and brine (100 mL). The organic phase was dried over sodium sulfate, filtered and concentrated *in vacuo*. The resulting residue was purified by column chromatography eluting with 0–40% ethyl acetate in petroleum ether to give ethyl 2-((2-(tert-butyl)-6-chlorobenzo[d]oxazol-7-yl)sulfonyl)-2-methylpropanoate (**78**, 10.3 g, 64% yield over two steps) as a white solid. LCMS(ESI) *m/z* 388 $[M+H]^+$.

Synthesis of 2-((2-(tert-butyl)-6-chlorobenzo[d]oxazol-7-yl)sulfonyl)-2-methylpropan-1-ol (79). To a solution of ethyl 2-((2-(tert-butyl)-6-chlorobenzo[d]oxazol-7-yl)sulfonyl)-2-methylpropanoate (**78**, 5.0 g) in THF (130 mL) under nitrogen at –50 °C was added DIBAL-H (1 M in hexane, 64.5 mL). The reaction mixture was allowed to warm to room temperature and stirred at room temperature for overnight. The reaction mixture was quenched with saturated ammonium chloride (20 mL), and then partitioned between ethyl acetate (150 mL) and sodium hydroxide solution (2 M, 150 mL). The organic phase was washed with saturated brine (150 mL), dried over sodium sulphate and evaporated *in vacuo* to give 2-((2-(tert-butyl)-6-chlorobenzo[d]oxazol-7-yl)sulfonyl)-2-methylpropan-1-ol (**79**, 4.5 g) as a white solid. LCMS(ESI) *m/z* 346 $[M+H]^+$.

Synthesis of 2-((2-(tert-butyl)-6-chlorobenzo[d]oxazol-7-yl)sulfonyl)-2-methylpropyl trifluoromethanesulfonate (80). To a solution of 2-((2-(tert-butyl)-6-chlorobenzo[d]oxazol-7-yl)sulfonyl)-2-methylpropan-1-ol (**79**, 5.2 g) in dichloromethane (100 mL) under nitrogen at room temperature was added pyridine (2.1 mL) and triflic anhydride (1 M in dichloromethane, 19.4 mL). The mixture was stirred at room temperature for 1 h, and then partitioned between dichloromethane (100 mL) and brine (100 mL). The organic phase was dried over anhydrous sodium sulphate and evaporated *in vacuo* to give 2-((2-(tert-butyl)-6-chlorobenzo[d]oxazol-7-

yl)sulfonyl)-2-methylpropyl trifluoromethanesulfonate (**80**, 6.5 g) as a white solid. LCMS(ESI) *m/z* 478 $[M+H]^+$.

Synthesis of 2-(tert-butyl)-6-chloro-7-((1-fluoro-2-methylpropan-2-yl)sulfonyl)benzo[d]oxazole (81). To a solution of 2-((2-(tert-butyl)-6-chlorobenzo[d]oxazol-7-yl)sulfonyl)-2-methylpropyl trifluoromethanesulfonate (**80**, 6.5 g) in THF (100 mL) at –15 °C was added TBAF (1 M in THF, 27.2 mL) dropwise. The reaction mixture was allowed to warm to 30 °C gradually and stirred for 2 h. The solvent was evaporated and the residue was partitioned between ethyl acetate (100 mL) and saturated brine (100 mL). The organic phase was dried over anhydrous sodium sulphate and evaporated *in vacuo*. The resulting residue was purified by column chromatography by eluting with 0–50% ethyl acetate in petroleum ether to afford 2-(tert-butyl)-6-chloro-7-((1-fluoro-2-methylpropan-2-yl)sulfonyl)benzo[d]oxazole (**81**, 2.4 g, 46% yield over three steps) as a white solid. LCMS(ESI) *m/z* 348 $[M+H]^+$.

Synthesis of 6-amino-3-chloro-2-((1-fluoro-2-methylpropan-2-yl)sulfonyl)phenol (82). To a solution of 2-(tert-butyl)-6-chloro-7-((1-fluoro-2-methylpropan-2-yl)sulfonyl)benzo[d]oxazole (**81**, 2.4 g) in 1,4-dioxane (20 mL) was added 37% HCl solution (20 mL). The reaction mixture was refluxed for 4 h, and then concentrated *in vacuo*. The residue was dissolved in ethyl acetate (20 mL) and the pH of the solution was adjusted to 8 with triethylamine. The organic phase was washed with brine (20 mL), dried over sodium sulphate, and concentrated *in vacuo*. The resulting residue was purified by column chromatography eluting with 0–80% ethyl acetate in petroleum ether to afford 6-amino-3-chloro-2-((1-fluoro-2-methylpropan-2-yl)sulfonyl)phenol (**82**, 1.9 g, 98% yield) as a white solid. ^{1}H NMR (400 MHz, $CDCl_3$) δ 10.18 (1 H, s), 6.89 (1 H, d, J = 8.8 Hz), 6.82 (1 H, d, J = 8.8 Hz), 4.62 (2 H, d, J = 41.6 Hz), 4.02 (2 H, br.s), 1.49 (6 H, s). LCMS(ESI) *m/z* 282 $[M+H]^+$.

Synthesis of 2-(tert-butyl)-6-chloro-7-((3-methyltetrahydrofuran-3-yl)sulfonyl)benzo[d]oxazole (84). To a solution of 2-(tert-butyl)-6-chloro-7-((tetrahydrofuran-3-yl)sulfonyl)benzo[d]oxazole (**83**, 4.3 g) and methyl iodide (2.0 mL) in THF (100 mL) at –70 ^{o}C was added LHMDS (1 M in THF, 31.3 mL). The reaction mixture was gradually warmed to room temperature and stirred at room temperature for 30 min. The reaction mixture was diluted with saturated NH_4Cl solution (100 mL) and extracted with ethyl acetate (2×150 mL). The combined organic layers were dried over sodium sulphate, filtered and concentrated *in vacuo* to afford 2-(tert-butyl)-6-chloro-7-((3-methyltetrahydrofuran-3-yl)sulfonyl)benzo[d]oxazole (**84**, 4.4 g). LCMS(ESI) *m/z* 358 $[M+H]^+$.

Synthesis of 6-amino-3-chloro-2-((3-methyltetrahydrofuran-3-yl)sulfonyl)phenol (85). To a solution of 2-(tert-butyl)-6-chloro-7-((3-methyltetrahydrofuran-3-yl)sulfonyl)benzo[d]oxazole (**84**, 4.4 g) in 1,4-dioxane (150 mL) was added 37% HCl solution (30.3 mL). The mixture was refluxed overnight, and then concentrated *in vacuo*. The residue was dissolved in ethyl acetate (100 mL). After pH of the solution was adjusted to 8 with saturated $NaHCO_3$ solution, the organic layer was washed with saturated brine, dried over sodium sulphate, filtered and concentrated *in vacuo*. The resulting residue was purified by column chromatography eluting with 0–80% ethyl acetate in petroleum ether to afford 6-amino-3-chloro-2-((3-methyltetrahydrofuran-3-yl)sulfonyl)phenol (**85**, 2.4 g, 66% yield over two steps). ^{1}H NMR (400 MHz, DMSO-d_6) δ 6.89–6.96 (2 H, m), 4.32 (1 H, d, J = 10.0 Hz), 3.76–3.89 (2 H, m), 3.60 (1 H, d, J = 10.0 Hz), 2.67 (1 H, dt, J = 13.3, 7.8 Hz), 1.93 (1 H, ddd, J = 13.1, 7.3, 5.3 Hz), 1.48 (3 H, s). LCMS(ESI) *m/z* 292 $[M+H]^+$.

Biology and DMPK. All studies were conducted in accordance with the GSK Policy on the Care, Welfare and Treatment of Laboratory Animals and were reviewed the Institutional Animal

Care and Use Committee either at GSK or by the ethical review process at the institution where the work was performed. The human biological samples were sourced ethically and their research use was in accord with the terms of the informed consents.

CXCR2 Tango Assay. The assay measures ligand-induced activation of the receptor CXCR2 in a stable cell line containing the recombinant human CXCR2 linked to a TEV protease site and a Gal4-VP16 transcription factor (Invitrogen). Ligand binding to the receptor results in the recruitment of arrestin proteins (tagged with protease) to the receptor and triggers the release of a tethered transcription factor. The transcription factor enters the nucleus and activates the transcription of the reporter gene. The ability of a compound to inhibit CXCR2 activation is indirectly assessed by measuring the reporter gene activity.

Cells were starved for 24 h at 37 ºC, 5% CO_2, harvested and re-suspended in assay medium at a density ~200,000 cells/mL. 50 nL/well of testing compounds in 100% DMSO solution were dispensed into the assay plate (Greiner 781090) using Echo 555 (Labcyte) with concentration-response program. The cell-free and un-stimulated control wells were loaded with 50 nL/well pure DMSO to ensure that the DMSO concentration was constant across the plate for all assays. 50 µL of assay medium, cell suspension without hCXCL1 (a CXCR2 ligand) and cell suspension with 80 nM hCXCL1 were added to cell-free control wells, un-stimulated control wells and the rest of wells, respectively. The cells were incubated overnight at 37 ºC/5% CO_2 and then 10 µL of 6× substrate mixture [LiveBLAzer™-FRET B/G substrate (CCF4-AM) Cat # K1096 from Invitrogen, Inc.] was dispensed into each well using Bravo and the plates were incubated at room temperature for another 2 h in the dark before reading on EnVision using one excitation channel (409 nm) and two emission channels (460 nm and 530 nm). The blue/green emission ratio (460 nm/530 nm) was calculated for each well, by dividing the cell-free background-subtracted Blue

emission values by the background-subtracted Green emission values. The concentration response curves were fitted based on sigmoidal concentration-response model to return IC_{50} and intrinsic activity (IA, percentage of maximum inhibition).

P-gp/BCRP Efflux Ratio (ER) and Cell Permeability Assay. Polarized Madin-Darby canine kidney (MDCKII) cells stably transfected with human P-gp (MDCKII-MDR1 cell line) were obtained from The Netherlands Cancer Institute (Amsterdam, The Netherlands). MDCKII-MDR1 cells transduced with BacMam2-BCRP according to experimental protocols reported previously were used for the in vitro transport studies in the Transwell system.[33b] The procedures of cell culture and transport studies were described previously.[33] The transport of test compounds (3 μM) was measured in duplicates in two directions [apical to basolateral (A → B) and basolateral to apical (B → A)] or one direction [apical to basolateral (A → B)] after 90 min incubation in the absence and presence of GF120918 (5 μM, a dual P-gp and BCRP inhibitor). The passive permeability (P_{exact}, nm/s) for test compounds across MDCKII monolayers were calculated using the equation reported previously.[33b] Efflux ratio (ER) is defined as the ratio of permeability of basolateral-to-apical to apical-to-basolateral direction in the absence of GF120918. The permeability ratio is defined as the ratio of permeability of apical-to-basolateral direction in the presence to absence of GF120918. The functionality of human P-gp and BCRP transporters in this *in vitro* system was qualified by typical ERs of amprenavir (a P-gp specific substrate) and dantrolene (a BCRP specific substrate) greater than 12 and 5, respectively.

Human Whole Blood CD11b Assay. The whole blood assay tested the compounds' ability to inhibit the upregulation of CD11b in GRO-α stimulated neutrophils in human whole blood. Blood was withdrawn by venipuncture from consented adults and poured into a Sterilin tube containing an anti-coagulant Heparin (10 uL/mL of blood). All the test compounds were

screened at a top 10 μM final assay concentration, (1 in 3 serial dilution to provide 10-point dose response curves) with a final DMSO concentration to 0.25% after addition of blood.

10 uL of blood was transferred to the compound plate using a multi-channel pipette, gently tapped and incubated for 15 min, at 37 ^{o}C. After 15 min, the stimulant GRO-α was diluted to 100 nM in 0.1% BSA (Albumin Bovine Serum)-PBS and 5 uL is dispensed across the whole plate for a final concentration of 33 nM. The plate was gently tapped and incubated further for 15 min at 37 ^{o}C. The plate was placed on ice for 1 min before addition of 10 uL of an antibody cocktail consisting of CD11b-FITC (40 μg/mL) purchased from BioLegend (address: Cambridge Bioscience, Munro House, Trafalgar Way, Bar Hill, Cambridge, UK) and CD16-PE purchased from BD Pharmingen (address: The Danby Building, Edmung Halley Road, Oxford Science Park, Oxford, UK) (stock concentration 100 tests, 2 mL stock volume is diluted 1 in 5). The plate was placed on ice for 1 h in the dark. The cells were then fixed using 200 μL/well of 1x FACS (Flow Activated Cell Sorting) Lyse solution (Becton and Dickinson-BD) and on ice for 20 min in the dark. The plate was centrifuged at 1600 rpm for 5 min and re-suspended with 200 μL of ice cold PBS. This step was repeated twice and on the final step the plate was re-suspended with 50 μL of ice cold PBS for flow cytometric analysis.

Samples were run on a Becton and Dickinson (BD)-Acurri C6 Flow Cytometer using a HyperCyt sampling apparatus (IntelliCyt) with a flow rate 2 μL/sec. CD11b upregulation is monitored in neutrophils and identified using a combination of both side scatter and CD16 expression.

Mouse Whole Blood CD11b Assay. 50 μL freshly isolated whole blood with anti-coagulant heparin (10 uL/mL of blood) from C57 mice was pretreated with CXCR2 compounds at concentrations from 1.5 nM to 10 μM in 96-U-well-plate (Corning, NY, US, Cat. #3799).

Samples were gently mixed with multi-channel pipette and incubated for 2 h in 37 °C incubator. 55 μL blood-compound mixture in each well was transferred into 96-V-well-plate (Corning, NY, US, Cat. #3897) for the secondary treatment with 100 nM murine CXCL1 (Pepro Tech, NJ, US, Cat. #250-11) in DPBS (ThermoFisher, PA, USA, Cat. #14190250)/0.1% BSA (Sigma, MO, US, Cat. #85040C). Samples were incubated for 10 min in 37 °C water bath with gentle agitation at 5 min. Then samples were placed on ice and fixed with 150 μL of ice cold CellFix solution (1% formaldehyde/0.1% azide/DPBS further 1:4 diluted in Robosep buffer from Stemcell Technologies, Vancouver, Canada, Cat. #20104) for 1 min. 50 μL of each sample was transferred to 96 V-well-plate preloaded with 5 μL anti-CD11b-FITC (ThermoFisher, PA, US, Cat. #11-0112-82) or isotype control of FITC-IgG2a (BD Biosciences, NJ, US, Cat. #553456). Samples were gently mixed and incubated for 20 min in the dark on ice. 200 μL freshly prepared 1×Red blood lysis buffer (BD Biosciences, NJ, US, Cat. #555899) was added into antibody-blood mixture for red blood cells lysis. This usually took 3–5 min. Samples were centrifuged at 1000 rpm for 5 min, and supernatant was discarded with replacement of 250 μL ice cold and sterile 1% FBS (ThermoFisher, PA, USA, Cat. #10099141)/DPBS.

Samples were gently mixed for FACS reading within 1hr with BD FACS Canto II flow cytometer and FACsDiva Software. CD11b population was analyzed by firstly gating on the granulocyte population on the FSC vs. SSC plot, and then gating on the CD16+ cells of neutrophil within the granulocyte population. As CD16+ cells usually take up 95% of granulocytes, this step is usually omitted. Therefore, mean FITC signal of granulocyte population subtracted by mean fluorescence of isotype control can reflect specific CD11b content.

Rat SOA for CNS Penetration. The blood brain barriers (BBB) separate the brain from the peripheral circulation. These barriers have tight junctions and also multiple efflux transporters to prevent CNS exposure of compounds to reach their CNS molecular targets. CNS penetration properties of CXCR2 compounds were evaluated in the male Han-Wistar rats after oral gavage at 2 mg/kg. Test compound was formulated as homogenous suspension in a dosing vehicle containing DMSO: 1% methylcellulose (w/v) = 1:99. At each time point post dose (0.25 h, 0.5 h, 1 h, 2 h, 4 h, 7 h), blood samples (> 60 µL/time point/each site) were collected via cardiac puncture, into separate EDTA-K_2 (0.5 M) containers following anaesthesia with isofluorane. Exact 50 uL of blood samples were diluted with 150 µL of diH_2O (1:3), snap frozen on dry ice and further stored at –80 °C. Immediately after blood collection, the brains from all the animals were excised, transferred suitable containers and immediately stored frozen. Brain were homogenized with 3-fold PBS (w/v) and further stored at –80 °C (dilution factor = 3.9).

Two separate calibration curves were prepared in blank blood/water mixture and brain homogenate respectively. Study samples and their corresponding calibration curves were extracted by protein precipitation. Exact 50 µL sample was aliquot into a clean extract plate and then extracted with 150 µL of acetonitrile containing analytical internal standard. After mixing and centrifugation, approximately 100 µL of supernatant was removed into an injection plate and sample was further diluted with same volume of deionized water. Quantitation of test compound was carried out by UPLC/MS/MS using an optimized methodology.

Systemic and brain exposure were estimated by AUC up to the last time point at 7 h. CNS penetration potential (K_p) of test compounds was evaluated from the ratio of AUC_{brain}/AUC_{blood}. $K_{p,uu}$ value was calculated using the measured K_p, free unbound compound fractions in blood and brain.

Air Pouch Model in Mouse and Rat. Air pouch model was induced with carrageenan in mouse and rat as described in previous studies with minor modifications.[36] In brief, 6-8 weeks male C57Bl/6 mice were anesthetized with pentobarbital and 5 ml sterile air was injected into the shaved back of each mouse on day 0. On day 3, 2.5 ml sterile air was used to re-inflate the pouch. Three days later (Day 6), another 2.5 ml sterile air was re-inflated. Similarly, air pouch model was induced in rat. 8-10 weeks male Wistar rats were used and 20 ml sterile air was injected for the first inflation, and 10 ml sterile air was injected for re-inflation on Day 3 and Day 6. In both mouse and rat air pouch model, 1 mL 2% carrageenan was injected into the pouch after the last air injection to induce inflammatory infiltration. 4 h after stimulation, the pouch was flushed with 4 mL PBS and exudates were collected for further analysis. Exudates were centrifuged and cell pellets were re-suspended and transfer to slides using cytospin. The slides were stained with Giemsa and total infiltrated cells and neutrophil were counted.

For compound testing, mice or rats were divided into four groups and orally treated with vehicle, or 1, 3, 10 mg/kg compound **68** orally BID from Day 3. On Day 6, vehicle and compound dosing were given immediately before air re-inflation and carrageenan induction. Whole blood was collected at 0 h, 1 h, and 4 h post compound treatment for PK analysis.

X-ray Diffraction Study. A solution of **68** in toluene was evaporated to obtain crystals that were suitable for study. Data were collected with an Oxford Diffraction Gemini A Ultra diffractometer at 175(2) K using Cu-Kα X-radiation (λ = 1.54178 Å). Crystal data and refinement summary: $C_{18}H_{23}ClN_2O_5S$; M = 414.89; colourless rod; 0.24 x 0.11 x 0.06 mm; orthorhombic; space group $P2_12_12_1$ (#19); a = 11.9118(2) Å, b = 15.4757(4) Å, c = 21.1168(5) Å, V = 3892.74(15) Å^3; Z = 8; D_{calc} = 1.416 Mgm^{-3}; θ_{max} = 66.78°; reflections collected = 13820; independent reflections = 6360; R_{int} = 0.0460; coverage = 97.7 %; restraints = 448; parameters =

621; S = 1.032; R_1 [$I>2\sigma(I)$] = 0.0388; wR_2 (all data) = 0.0956; absolute structure parameter = 0.007(13); and largest difference peak and hole = 0.281 and -0.278 eÅ^{-3}. A description of the refinement, a further discussion on the assignment of the absolute configuration and the full tables associated with the crystal structure are given in the Supporting Information. A crystallographic information file has been deposited with the Cambridge Crystallographic Data Centre. CCDC 1810782 contains the supplementary crystallographic data for this paper. The data can be obtained free of charge from The Cambridge Crystallographic Data Centre via www.ccdc.cam.ac.uk/structures.

ASSOCIATED CONTENT

Supporting Information. The following files are available free of charge.

Detailed synthetic procedures for compounds **9**–**39**, **41**–**65**, **67**, **69**–**71**, **35'**–**38'** and spectral data for the compounds (PDF)

Molecular formula strings and some *in vitro* data (CSV)

AUTHOR INFORMATION

Corresponding Author

* To whom correspondence should be addressed. Phone: +86-21-61590721. Fax: +86-21-61590730. Email: feng.q.ren@gsk.com; 2648666968@qq.com

Author Contributions

The manuscript was written through contributions of all authors. All authors have given approval to the final version of the manuscript.

Notes

All the authors are/were employees of GlaxoSmithKline, a global healthcare company that may conceivably benefit financially through this publication.

ACKNOWLEDGMENT

We thank Professor W. Clegg and Dr. M. R. Probert for the GSK-funded crystal structure of **68**.

ABBREVIATIONS

AD, Alzheimer's disease; AUC, area under curve; BCRP, breast cancer resistance protein; BID, twice a day; CCR2, C-C chemokine receptor type 2; CF, cystic fibrosis; CNS, central nervous system; COPD, chronic obstructive pulmonary disease; CXCL1, C–X–C motif ligand 1; CXCL8, C–X–C motif ligand 8; CXCR2, C–X–C chemokine receptor type 2; DNAUC, dose normalized area under curve; *ee*, enantiomeric excess; EWG, electron withdrawing group; FaSSIF, fasted state simulated intestinal fluids; GPCR, G-protein-coupled receptor; Gro-α, growth-related oncogene-alpha; HWB, human whole blood; ICB, immune checkpoint blockage; IL-8, interleukin 8; IV, intravenous; LHS, left-hand-side; LTP, long-term potentiation; MS, multiple sclerosis; MW, molecular weight; NK cells, natural killer cells; PFI, property forecast index; P-gp, P-glycoprotein; PK, pharmacokinetics; PMN, polymorphonuclear leukocyte; RA, rheumatoid arthritis; RHS, right-hand-side; SAR, structure-activity relationship; SFC, supercritical fluid chromatography; SOA, short oral absorption; $T_{1/2}$, half-life.

REFERENCES

1. Anika, S.; Alexander, Z. CXCR2: From bench to bedside. *Front. Immunol.* **2012**, *3*, 263.
2. Holz, O.; Khalilieh, S.; Ludwig-Sengpiel, A.; Watz, H.; Stryszak, P.; Soni, P.; Tsai, M.; Sadeh, J.; Magnussen, H. SCH527123, a novel CXCR2 antagonist, inhibits ozone-induced neutrophilia in healthy subjects. *Eur. Respir. J.* **2010**, *35* (3), 564-570.
3. Aul, R.; Patel, S.; Summerhill, S.; Kilty, I.; Plumb, J.; Singh, D. LPS challenge in healthy subjects: an investigation of neutrophil chemotaxis mechanisms involving CXCR1 and CXCR2. *Int. Immunopharmacol.* **2012**, *13* (3), 225-231.
4. Breland, U. M.; Halvorsen, B.; Hol, J.; Øie, E.; Paulsson-Berne, G.; Yndestad, A.; Smith, C.; Otterdal, K.; Hedin, U.; Wæhre, T.; Sandberg, W. J.; Frøland, S. S.; Haraldsen, G.; Gullestad, L.; Damås, J. K.; Hansson, G. K.; Aukrust, P. A potential role of the CXC chemokine GRO[alpha] in atherosclerosis and plaque destabilization: downregulatory effects of statins. *Arterioscler. Thromb. Vasc. Biol.* **2008**, *28* (5), 1005-1011.
5. Boppana, N. B.; Devarajan, A.; Gopal, K.; Barathan, M.; Bakar, S. A.; Shankar, E. M.; Ebrahim, A. S.; Farooq, S. M. Blockade of CXCR2 signalling: a potential therapeutic target for preventing neutrophil-mediated inflammatory diseases. *Exp. Biol. Med.* **2014**, *239* (5), 509-518.
6. a) Miller, B. E.; Mistry, S.; Smart, K.; Connolly, P.; Carpenter, D. C.; Cooray, H.; Bloomer, J. C.; Tal-Singer, R.; Lazaar, A. L. The pharmacokinetics and pharmacodynamics of Danirixin (GSK1325756) – a selective CXCR2 antagonist – in healthy adult subjects. *BMC Pharmacol. Toxicol.* **2015**, *16*, 1-12. b) Rennard, S. I.; Dale, D. C.; Donohue, J. F.; Kanniess, F.; Magnussen, H.; Sutherland, E. R.; Watz, H.; Lu, S.; Stryszak, P.; Rosenberg, E.; Staudinger, H. CXCR2 antagonist MK-7123. a phase 2

proof-of-concept trial for chronic obstructive pulmonary disease. *Am. J. Respir. Crit. Care Med.* **2015**, *191* (9), 1001-1011.

7. Koch, A. E.; Kunkel, S. L.; Shah, M. R.; Hosaka, S.; Halloran, M. M.; Haines, G. K.; Burdick, M. D.; Pope, R. M.; Strieter, R. M. Growth-related gene product alpha. A chemotactic cytokine for neutrophils in rheumatoid arthritis. *J. Immunol.* **1995**, *155* (7), 3660-3666.
8. Steele, C. W.; Karim, S. A.; Leach, J. D. G.; Bailey, P.; Upstill-Goddard, R.; Rishi, L.; Foth, M.; Bryson, S.; McDaid, K.; Wilson, Z.; Eberlein, C.; Candido, J. B.; Clarke, M.; Nixon, C.; Connelly, J.; Jamieson, N.; Carter, C. R.; Balkwill, F.; Chang, D. K.; Evans, T. R. J.; Strathdee, D.; Biankin, A. V.; Nibbs, R. J. B.; Barry, S. T.; Sansom, O. J.; Morton, J. P. CXCR2 inhibition profoundly suppresses metastases and augments immunotherapy in pancreatic ductal adenocarcinoma. *Cancer Cell*, **2016**, *29*, 1-14.
9. Lu, X.; Horner, J. W.; Paul, E.; Shang, X.; Troncoso, P.; Deng, P.; Jiang, S.; Chang, Q.; Spring, D. J.; Sharma, P.; Zebala, J. A.; Maeda, D. Y.; Wang, Y. A.; DePinho, R. A. Effective combinatorial immunotherapy for castration-resistant prostate cancer. *Nature*, **2017**, *543*, 728-732.
10. Yang, L.; Liu, Z.; Wu, R.; Yao, Q.; Gu Z.; Liu, M. Correlation of C-X-C chemokine receptor 2 upregulation with poor prognosis and recurrence in human glioma. *Onco Targets Ther.* **2015**, *8*, 3203-3209.
11. a) Veenstra, M.; Ransohoff, R. M. Chemokine receptor CXCR2: physiology regulator and neuroinflammation controller? *J. Neuroimmunol.* **2012**, *246* (1-2), 1-9. b) Semple, B. D.; Kossmann, T.; Morganti-Kossmann, M. C. Role of chemokines in CNS health and pathology: a focus on the CCL2/CCR2 and CXCL8/CXCR2 networks. *J. Cereb. Blood*

Flow Metab. **2010**, *30* (3), 459-473. c) Melik-Parsadaniantz, S.; Rostene, W. Chemokines and neuromodulation. *J. Neuroimmunol.* **2008**, *198* (1-2), 62-68.

12. Du, C. S.; Xie, X. G protein-coupled receptors as therapeutic targets for multiple sclerosis. *Cell Res.* **2012**, *22* (7), 1108-1128.
13. Zhang, X.-F.; Zhao, Y.-F.; Zhu, S.-W.; Huang, W.-J.; Luo, Y.; Chen, Q.-Y.; Ge, L.-J.; Li, R.-S.; Wang, J.-F.; Sun, M.; Xiao, Z.-C.; Fan, G.-H. CXCL1 triggers caspase-3 dependent tau cleavage in long-term neuronal cultures and in the hippocampus of aged mice: implications in Alzheimer's disease. *J. Alzheimers Dis.* **2015**, *48* (1), 89-104.
14. Zhang, Z.-J.; Cao, D.-L.; Zhang, X.; Ji, R.-R.; Gao, Y.-J. Chemokine contribution to neuropathic pain: respective induction of CXCL1 and CXCR2 in spinal cord astrocytes and neurons. *Pain* **2013**, *154* (10), 2185-2197.
15. White, J. R.; Lee, J. M.; Young, P. R.; Hertzberg, R. P.; Jurewicz, A. J.; Chaikin, , M. A.; Widdowson, K.; Foley, J. J.; Martin, L. D.; Griswold, D. E.; Sarau, H. M. Identification of a potent, selective non-peptide CXCR2 antagonist that inhibits interleukin-8-induced neutrophil migration. *J. Biol. Chem*. **1998**, *273* (17), 10095-10098.
16. a) Bertini, R.; Allegretti, M.; Bizzarri, C.; Moriconi, A.; Locati, M.; Zampella, G.; Cervellera, M. N.; di Cioccio, V.; Cesta, M. C.; Galliera, E.; Martinez, F. O.; Bitondo, R. D.; Troiani, G.; Sabbatin, V.; D'Anniballe, G.; Anacardio, R.; Cutrin, J. C.; Cavalieri, B.; Mainiero, F.; Strippoli, R.; Villa, P.; Girolamo, M. D.; Martin, F.; Gentile, M.; Santoni, A.; Corda, D.; Poli, G.; Mantovani, A.; Ghezzi, P.; Colotta, F. Noncompetitive allosteric inhibitors of the inflammatory chemokine receptors CXCR1 and CXCR2: Prevention of reperfusion injury. *PNAS.* **2004**, *101* (32), 11791-11796. b) Chapman, R. W.; Phillips, J. E.; Hipkin, R. W.; Curran, A. K.; Lundell, D.; Fine, J. S. CXCR2 antagonists for the

treatment of pulmonary disease. *Pharmacol. Ther.* **2009**, *121* (1), 55-68. c) Opfermann, P.; Derhaschnig, U.; Felli, A.; Wenisch, J.; Santer, D.; Zuckermann, A.; Dworschak, M.; Jilma, B.; Steinlechner, B. A pilot study on reparixin, a CXCR1/2 antagonist, to assess safety and efficacy in attenuating ischaemia-reperfusion injury and inflammation after on-pump coronary artery bypass graft surgery. *Clin. Exp. Immunol.* **2015**, *180* (1), 131-142.

17. Nicholls, D. J.; Wiley, K.; Dainty, I.; MacIntosh, F.; Phillips, C.; Gaw, A.; Mårdh, C. K. Pharmacological characterization of AZD5069, a slowly reversible CXC chemokine receptor 2 antagonist. *J. Pharm. Exp. Ther.* **2015**, *353* (2), 340-350.
18. Walters, I.; Austin, C.; Austin, A.; Bonnert, R.; Cage, P.; Christie, M.; Ebden, M.; gardiner, S.; Grahames, C.; Hill, S.; Hunt, F.; Jewell, R.; Lewis, S.; Martin, I.; Nicholls, D.; Robinson, D. Evaluation of a series of bicyclic CXCR2 antagonists. *Bioorg. Med. Chem. Lett.* **2008**, *18* (2), 798-803.
19. Gonsiorek, W.; Fan, X.; Hesk, D.; Fossetta, J.; Qiu, H.; Jakway, J.; Billah, M.; Dwyer, M.; Chao, J.; Deno, G.; Taveras, A.; Lundell, D. J.; Hipkin, R. W. Pharmacological characterization of Sch527123, a potent allosteric CXCR1/CXCR2 antagonist. *J. Pharm. Exp. Ther.* **2015**, *322* (2), 477-485.
20. Rennard, S. I.; Dale, D. C.; Donohue, J. F.; Kanniess, F.; Magnussen, H.; Sutherland, E. R.; Watz, H.; Lu, S.; Stryszak, P.; Rosenberg, E.; Staudinger, H. CXCR2 antagonist MK-7123: a phase 2 proof-of-concept trial for chronic obstructive pulmonary disease. *Am. J. Respir. Crit. Care Med.* **2015**, *191* (9), 1001-1011.
21. Ning, Y.; Labonte, M. J.; Zhang, W.; Bohanes, P. O.; Gerger, A.; Yang, D.; Benhaim, L.; Paez, D.; Rosenberg, D. O.; Nagulapalli V., Kalyan C.; Louie, S. G.; Petasis, N. A.;

Ladner, R. D.; Lenz, H.-J. The CXCR2 antagonist, SCH-527123, shows antitumor activity and sensitizes cells to oxaliplatin in preclinical colon cancer models. *Mol. Cancer Ther.* **2012**, *11* (6), 1353-1364.

22. Porter, D. W.; Bradley, M.; Brown, Z.; Charlton, S. J.; Cox, B.; Hunt, P.; Janus, D.; Lewis, S.; Oakley, P.; O'Connor, D.; Reilly, J.; Smith, N.; Press, N. J. The discovery of potent, orally bioavailable pyrimidine-5-carbonitrile-6-alkyl CXCR2 receptor antagonists. *Bioorg. Med. Chem. Lett.* **2014**, *24* (15), 3285-3290.
23. Li, J. J.; Carson, K. G.; Trivedi, B. K.; Yue, W. S.; Ye, Q.; Glynn, R. A.; Miller, S. R.; Connor, D. T.; Roth, B. D.; Luly, J. R.; Low, J. E.; Heilig, D. J.; Yang, W.; Qin, S.; Hunt, S. Synthesis and structure-activity relationship of 2-amino-3-heteroaryl-quinoxalines as non-peptide, small-molecule antagonists for interleukin-8 receptor. *Bioorg. Med. Chem.* **2003**, *11* (17), 3777-3790.
24. Schuler, A. D.; Engles, C. A.; Maeda, D. Y.; Quinn, M. T.; Kirpotina, L. N.; Wicomb, W. N.; Mason, S. N.; Auten, R. L.; Zebala, J. A. Boronic acid-containing aminopyridine- and aminopyrimidinecarboxamide CXCR1/2 antagonists: Optimization of aqueous solubility and oral bioavailability. *Bioorg. Med. Chem. Lett.* **2015**, *25* (18), 3793-3797.
25. a) Traves, S. L.; Smith, S. J.; barnes, P. J.; Donnelly, L. E. Specific CXC but not CC chemokines cause elevated monocyte migration in COPD: a role for CXCR2. *J. Leukoc. Biol.* **2004**, *76* (2), 441-450. b) Ryu, J. K.; Cho, T.; Choi, H. B.; Jantaratnotai, N.; McLarnon, J. G. Pharmacological antagonism of interleukin-8 receptor CXCR2 inhibits inflammatory reactivity and is neuroprotective in an animal of Alzeimer's disease. *J. Neuroinflamm.* **2015**, 12:144. c) Busch-Petersen, J. Small molecule antagonists of the

CXCR2 and CXCR1 chemokine receptors as therapeutic agents for the treatment of inflammatory diseases. *Curr. Top. Med. Chem.* **2006**, *6*, 1345-1352.

26. Lazaar, A. L.; Sweeney, L. E.; MacDonald, A. J.; Alexis, N. E.; Chen, C.; Tal-Singer, R. SB-656933, a novel CXCR2 selective antagonist, inhibits ex vivo neutrophil activation and ozone-induced airway inflammation in humans. *Br. J. Clin. Pharmacol.* **2011**, *72* (2), 282-293.
27. a) Miller, B. E.; Mistry, S.; Smart, K.; Connolly, P.; Carpenter, D. C.; Cooray, H.; Bloomer, J. C.; Tal-Singer, R.; Lazaar, A. L. The pharmacokinetics and pharmacodynamics of danirixin (GSK1325756) - a selective CXCR2 antagonist - in healthy adult subjects. *BMC Pharmacol. Toxicol.* **2015**, *16*, 1-12. b) Dwyer, M. P.; Yu, Y. CXCR2 modulators: a patent review (2009 – 2013). *Expert Opin. Ther. Patents* **2014**, *24* (5), 519-534.
28. a) Ha, H.; Debnath, B.; Neamati, N. Role of the CXCL8-CXCR1/2 axis in cancer and inflammatory diseases. *Theranostics.* **2017**, *7* (6), 1543-1587, and references therein. b) Busch-Petersen, J.; Wang, Y. Phenol-containing antagonists of the CXCR2 receptor. *Expert Opin. Ther. Patents*, **2008**, *18 (6)*, 629-637.
29. Xu, H.; Lu, H.; Xu, Z.; Luan, L.; Li, C.; Xu, Y.; Dong, K.; Zhang, J.; Li, X.; Li, Y.; Liu, G.; Gong, S.; Zhao, Y.-G.; Liu, A.; Zhang, Y.; Zhang, W.; Cai, X.; Xiang, J.-N.; Elliott, J. D.; Lin, X. Discovery of CNS penetrant CXCR2 antagonists for the potential treatment of CNS demyelinating disorders. *ACS Med. Chem. Lett.* **2016**, *7* (4), 397-402.
30. Young, R. J.; Green, D. V.S.; Luscombe, C. N.; Hill, A. P. Getting physical in drug discovery II: the impact of chromatographic hydrophobicity measurements and aromaticity. *Drug Discov. Today* **2011**, *16*, 822-830.

31. Unpublished result.

32. Busch-Petersen, J. IL-8 Receptor Antagonists. US 20070249672A1, Oct 25, 2007.

33. a) Liu, H.; Yu, N.; Lu, S.; Ito, S.; Zhang, X.; Prasad, B.; He, E.; Lu, X.; Li, Y.; Wang, F.; Xu, H.; An, G.; Unadkat, J. D.; Kusuhara, H.; Sugiyama, Y.; Sahi, J. Solute carrier family of the organic anion-transporting polypeptides 1A2-Madin-Darby Canine Kidney II: a promising in vitro system to understand the role of organic anion-transporting polypeptide 1A2 in blood-brain barrier drug penetration. *Drug Metab. Dispos.* **2015**, *43* (7), 1008-1018. b) Liu, H.; Huang, L.; Li, Y.; Fu, T.; Sun, X.; Zhang, Y. Y.; Gao, R.; Chen, Q.; Zhang, W.; Sahi, J.; Summerfield, S.; Dong, K. Correlation between membrane protein expression levels and transcellular transport activity for breast cancer resistance protein. *Drug Metab. Dispos.* **2017**, *45* (5), 449-456.

34. Clarysse, S.; Brouwers, J.; Tack J.; Annaert, P.; Augustijns, P. Intestinal drug solubility estimation based on simulated intestinal fluids: comparison with solubility in human intestinal fluids. *Eur. J. Pharm. Sci*. **2011**, *43* (4), 260-269.

35. Hammarlund-Udenaes, M.; Fridén, M.; Syvänen, S.; Gupta, A. On the rate and extent of drug delivery to the brain. *Pharm. Res*. **2008**, *25* (8), 1737-1750.

36. a) Sin, Y. M.; Sedgwick, A. D.; Chea, E. P.; Willoughby, D. A. Mast cells in newly formed lining tissue during acute inflammation: a six-day air pouch model in the mouse. *Ann. Rheum. Dis.* **1986**, *45*, 873-877. b) Romano, M.; Faggioni, R.; Sironi, M.; Sacco, S.; Echtenacher, B.; Di Santo, E.; Salmona, M.; Ghezzi, P. Carrageenan-induced acute inflammation in the mouse air pouch synovial model. Role of tumor necrosis factor. *Mediators Inflamm*. **1997**, *6*, 32-38. c) Martin S. W.; Stevens, A. J.; Brennan, B. S.; Davies, D.; Rowland, M.; Houston, J. B. The six-day-old rat air pouch model of

inflammation: characterization of the inflammatory response to carrageenan. *J. Pharmacol. Toxicol. Methods* **1994**, *32*, 139-147. d) Hambelton, P.; Miller, P. Studies on carrageenan air pouch inflammation in the rat. *Br. J. Exp. Path.* **1989**, *70*, 425-433.

37. a) Corey, E. J.; Bakshi, R. K.; Shibata, S. Highly enantioselective borane reduction of ketones catalyzed by chiral oxazaborolidines. Mechanism and synthetic implications. *J. Am. Chem. Soc.* **1987**, *109*, 5551-5553. b) Corey, E. J.; Bakshi, R. K.; Shibata, S.; Chen, C. P.; Singh, V. K. A stable and easily prepared catalyst for the enantioselective reduction of ketones. Applications to multistep syntheses. *J. Am. Chem. Soc.* **1987**, *109*, 7925-7926.

FIGURES.

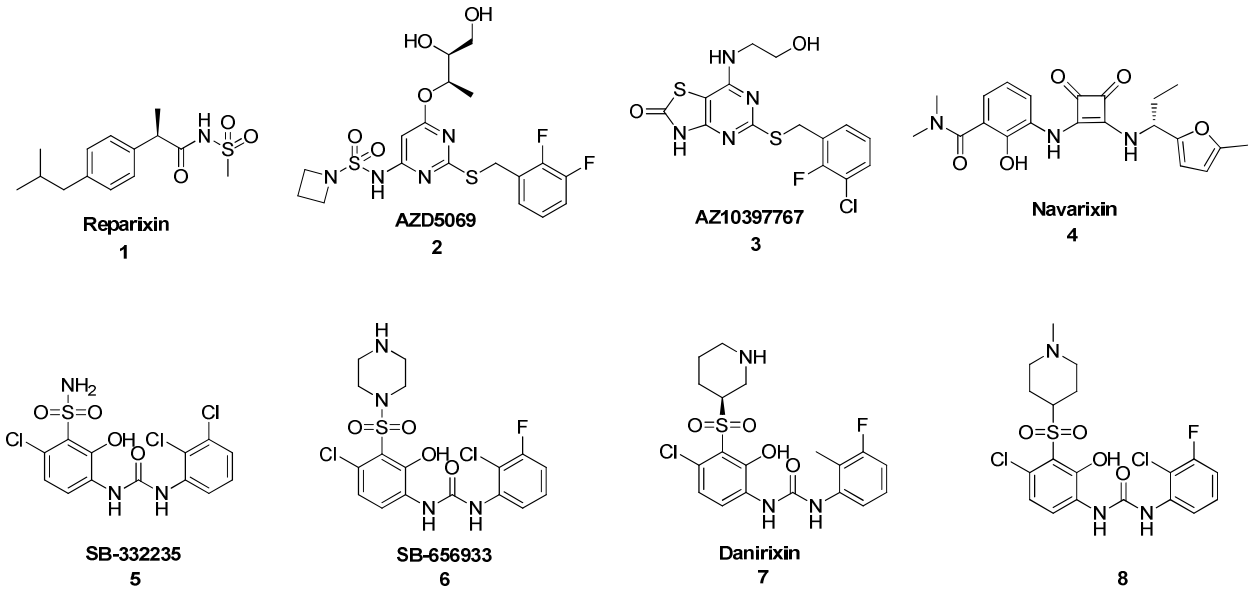

Figure 1. Structures of representative small molecule CXCR2 antagonists.

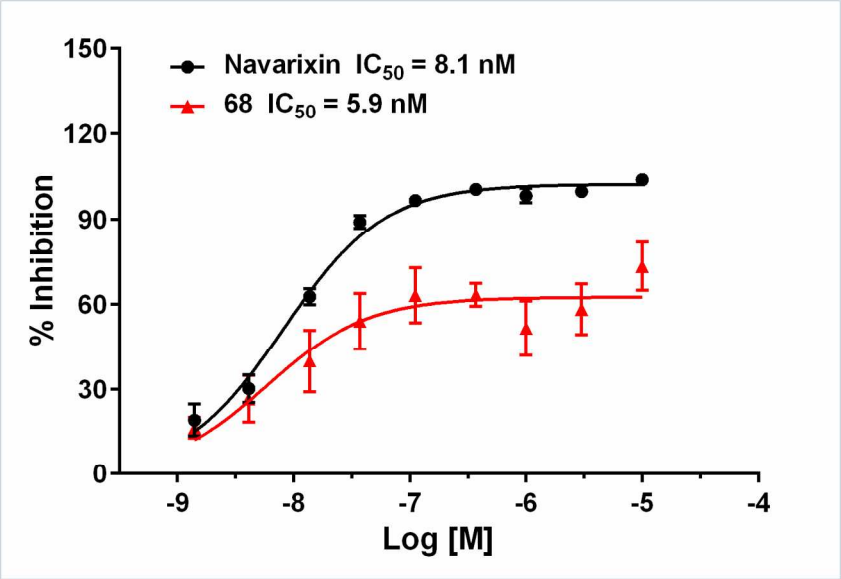

Figure 2a. Mouse whole blood CD11b assay of compound **68**.

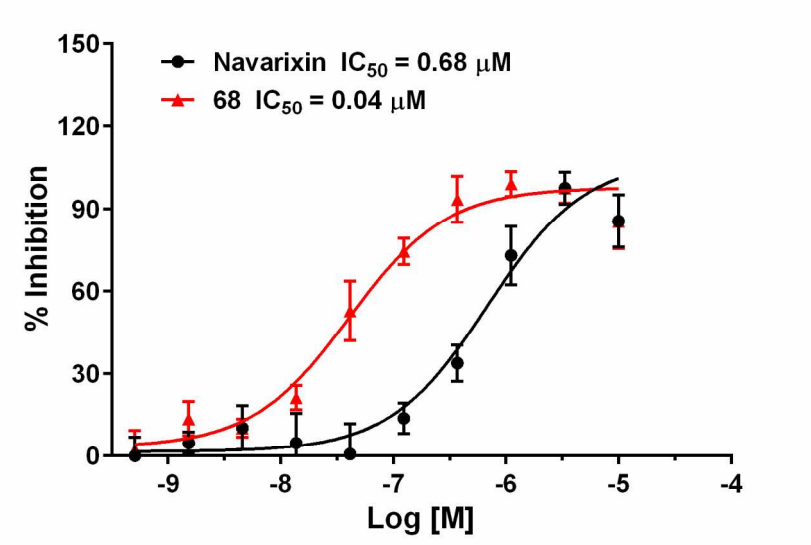

Figure 2b. Human whole blood CD11b assay of compound **68**.

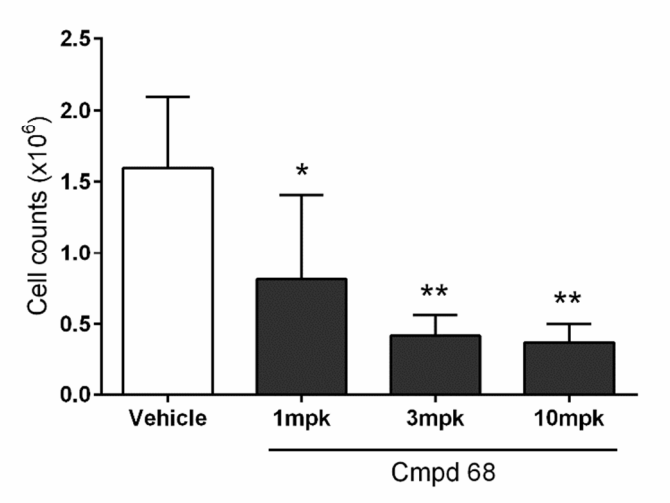

Figure 3a. Compound **68** inhibited neutrophil migration to the air pouch in mouse. The neutrophil cell number in the lavage were counted after 4 hours carageenan induction, the percentage were calculated compared to vehicle group. * $p<0.05$, ** $p<0.01$, compared with the vehicle group. One-way ANOVA, followed by Bonferroni Multiple Comparison Test.

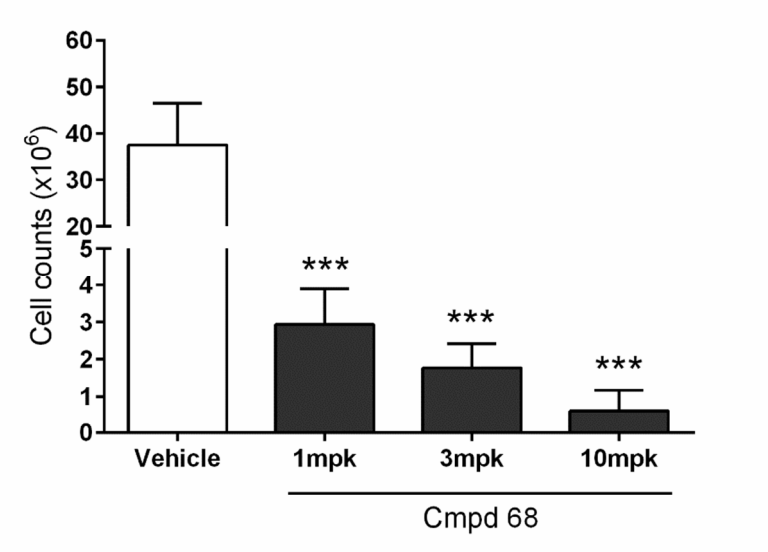

Figure 3b. Compound **68** inhibited neutrophil migration to air pouch in rat. The neutrophil cell number in the lavage were counted after 4 hours carageenan induction, the percentage were calculated compared to vehicle group. *** $p<0.001$ indicates significantly decreasing compared with the vehicle group. One-way ANOVA, followed by Dunnett's Multiple Comparison Test.

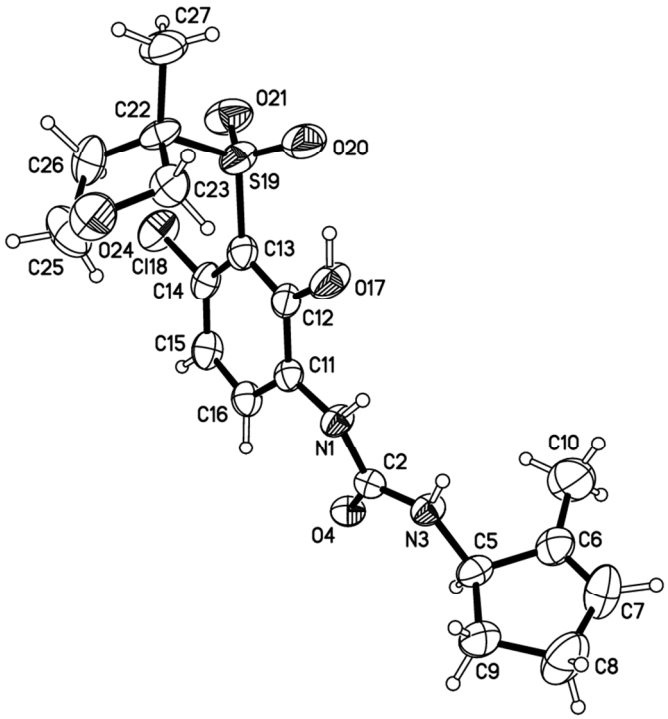

Figure 4. A view of one of the independent molecules from the crystal structure of **68**, showing the numbering scheme employed (the second molecule is numbered in an analogous fashion, from N31 to C57). Anisotropic atomic displacement ellipsoids for the non-hydrogen atoms are shown at the 50% probability level. For clarity, only one of the two disorder components for the 3-methyltetrahydrofuran-3-yl group is shown. Hydrogen atoms are displayed with an arbitrarily small radius.

SCHEMES.

Scheme 1. Retro-synthetic Analysis and Synthesis of RHS Intermediate **75**[a]

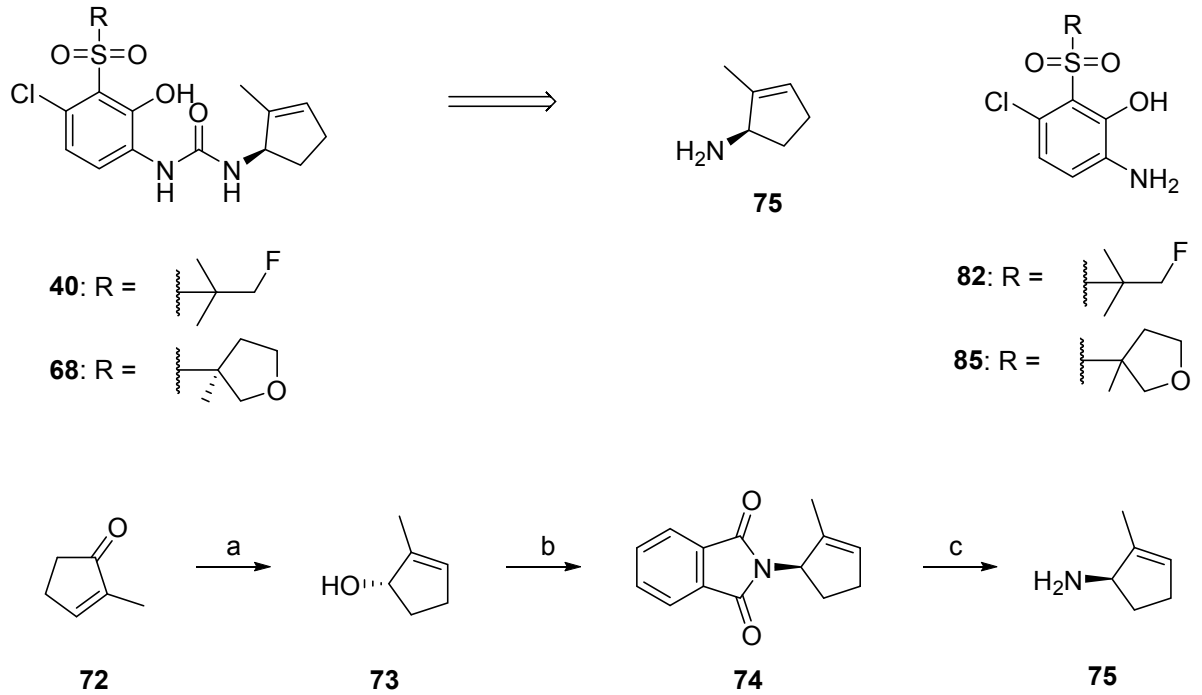

[a]Reagents and conditions. a) (*R*)-CBS, BH_3·THF, THF, –60 °C; b) phthalimide, PPh_3, DIAD, THF, 0 °C, 28% over two steps; c) hydrazine, EtOH, reflux, 100%.

Scheme 2. Synthesis of Lead Compound **40**[a]

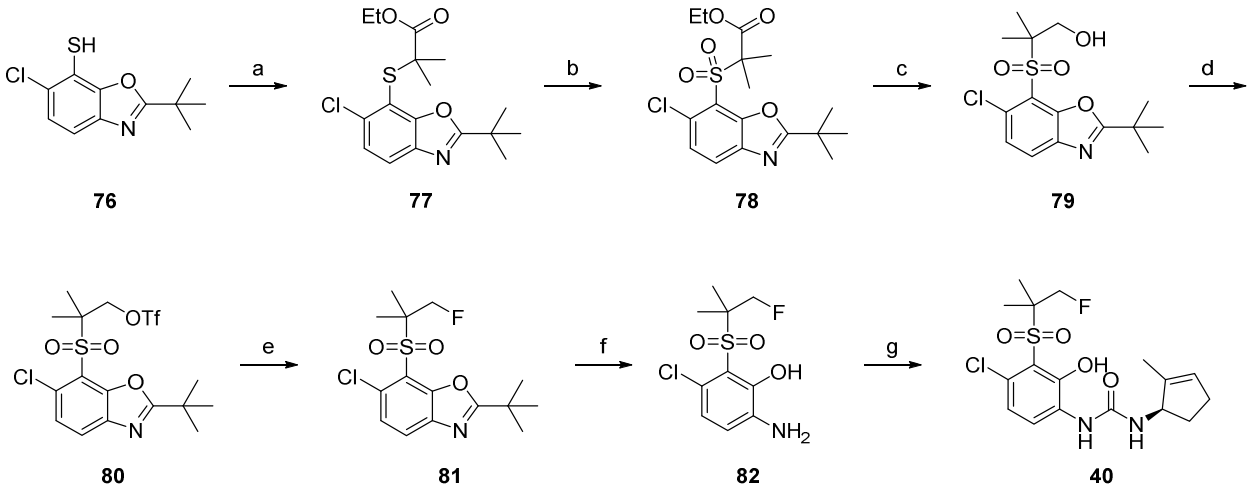

[a]Reagents and conditions. a) ethyl 2-bromo-2-methylpropanoate, K_2CO_3, DMF, 60 °C; b) *m*-CPBA, DCM, rt, 64% over two steps; c) DIBAL-H, THF, –50 °C → rt; d) triflic anhydride,

pyridine, DCM, rt; e) TBAF, THF, –15 °C → 30 °C, 46% over three steps; f) 37% HCl, dioxane, reflux, 98%; g) (i) **75**, triphosgene, $NaHCO_3$, DCM, 0 °C → rt, (ii) pyridine, rt, 58%.

Scheme 3. Synthesis of Lead Compound **68**[a]

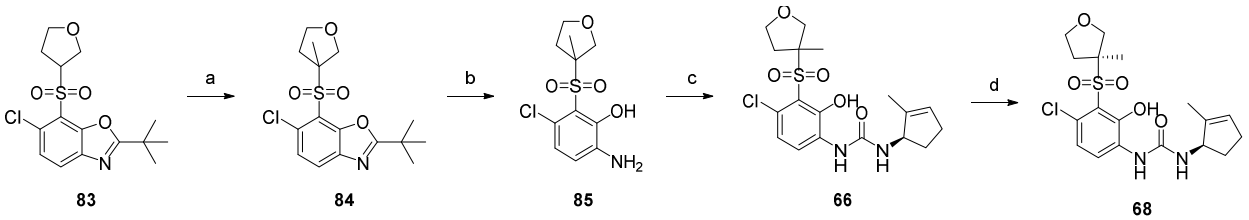

[a]Reagents and conditions. a) LiHMDS, MeI, THF, –70 °C → rt; b) 37% HCl, Dioxane, reflux, 66% over two steps; c) (i) **75**, triphosgene, $NaHCO_3$, DCM, 0 °C → rt, (ii) pyridine, 40 °C, 96%; d) chiral SFC separation, 22%.

TABLES

Table 1. SAR of the R Group to Replace the 2-Chloro-3-fluorophenyl Aromatic Ring with Alaphatic Rings[a]

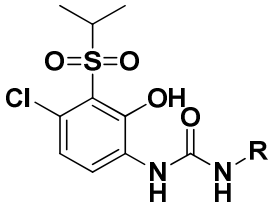

9–34

Cmpd	R	MW/PFI[b]	CXCR2 Tango pIC_{50}[c]	Cmpd	R	MW/PFI[b]	CXCR2 Tango pIC_{50}[c]
9	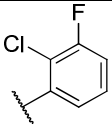	421/8.2	9.4	**22**	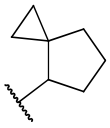	387/7.0	7.4
10	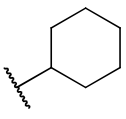	375/6.7	7.3	**23**	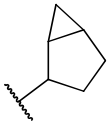	373/6.2	7.6

11	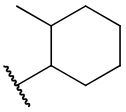	389/7.3[d]	6.5	**24**	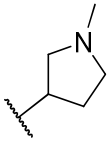	376/2.1	<5
12	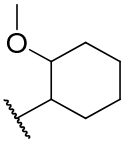	405/6.4	5.8	**25**	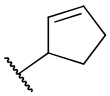	359/5.5[d]	8.2
13	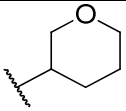	377/4.4	6.2	**26**	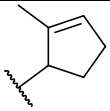	373/6.4	9.4
14	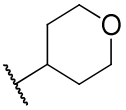	377/4.3[d]	5.9	**27**	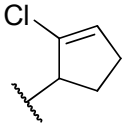	393/6.0	9.0
15	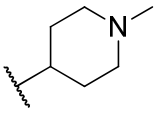	390/2.7[d]	<5	**28**	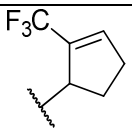	427/6.5	7.6
16	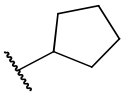	361/6.0	8.0	**29**	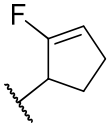	377/5.7	8.0
17	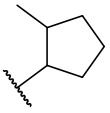	375/6.8	8.0	**30**	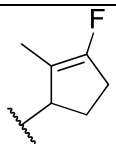	391/5.9[d]	8.8
18	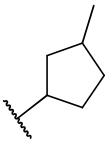	375/6.7	6.7	**31**	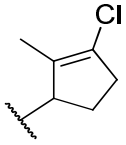	407/7.1	8.5
19	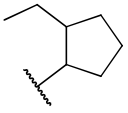	389/6.8[d]	7.2	**32**	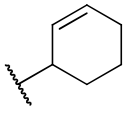	373/6.4	8.0
20	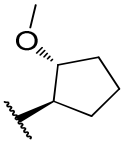	391/5.1	6.6	**33**	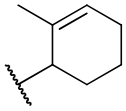	387/7.1	7.9

21	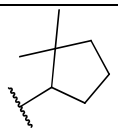	389/6.9[d]	6.8	**34**	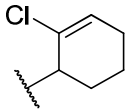	407/6.6[d]	8.0

[a]All compounds except for **9**, **10**, **14**, **15**, and **16** were prepared and tested as racemates. Detailed synthetic procedures are described in the Experimental Section. [b]PFI = Chrom $logD_{pH7.4}$ + # Ar, and Chrom $logD_{pH7.4}$ was measured.[30] [c]CXCR2 Tango assay pIC_{50} value is the average of at least two measurements. [d]Using predicted $logD_{pH7.4}$ value from ACD software, version 11.0.

Table 2. Comparisons Between *(R)*- and *(S)*-isomers[a]

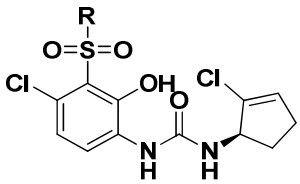

35–38

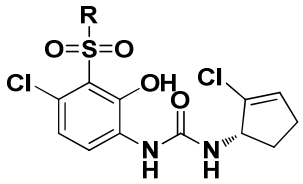

35'–38'

R	Cmpd	CXCR2 Tango pIC_{50}[b]	Cmpd	CXCR2 Tango pIC_{50}[b]
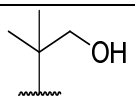	**35**	8.4	**35'**	6.3
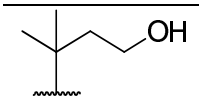	**36**	9.6	**36'**	7.1
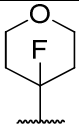	**37**	9.3	**37'**	7.0
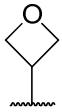	**38**	6.5	**38'**	5.6

[a]All compounds were prepared and tested as known single *(R)*- or *(S)*-enantiomers. Detailed synthetic procedures are described in the Supporting Information. [b]CXCR2 Tango assay pIC_{50} value is the average of at least two measurements.

Table 3. Selected SAR of LHS R^1 and R^2 Exploration[a]

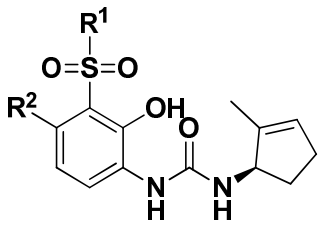

39–53

Cmpd	R^1	R^2	MW/PFI[b]	CXCR2 Tango pIC_{50}[c]	FaSSIF sol. (μg/mL)[d]	P-gp/BCRP efflux ratio[e]	Perm. (nm/s)	HWB CD11b pIC_{50}
39	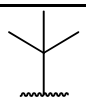	Cl	387/7.4	9.0	1.2	1.5[f]	364	6.5
40	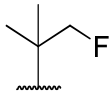	Cl	405/6.6	9.2	3.0	0.87	654	7.0
41	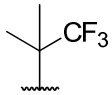	Cl	441/6.7	9.3	3.4	1.6[f]	339	N.D.
42	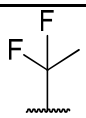	Cl	395/4.3	9.4	50.8	2.4[f]	348	6.2
43	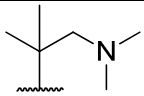	Cl	430/4.8	6.9	395.4	N.D.	N.D.	N.D.
44	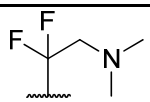	Cl	438/4.5	8.7	128.1	12.6	266	6.2
45	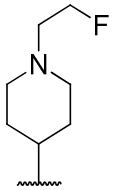	Cl	460/5.4	9.2	287.5	7.3	212	6.7

46	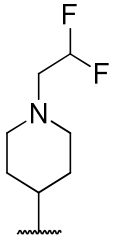	Cl	478/6.1	8.6	59.0	9.4	177	N.D.
47	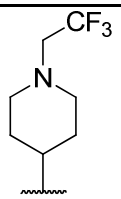	Cl	496/5.9[g]	6.5	N.D.	N.D.	N.D.	N.D.
48	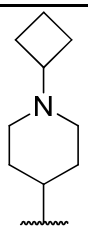	Cl	468/4.4[g]	9.4	491.1	3.3	320	6.3
49	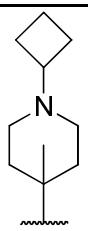	Cl	482/6.6	8.4	139.3	N.D.	N.D.	N.D.
50	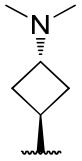	Cl	428/3.7	9.0	387.2	3.4[f]	203	6.9
51		Cl	454/3.7	9.0	757.6	2.8[f]	205	7.0
52	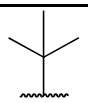	CN	377/4.1	9.7	685.6	4.0[f]	90	6.8
53	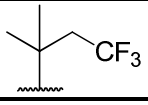	CN	431/4.3	9.8	407.9	4.3[f]	30	6.0

[a]All compounds were prepared and tested as known single *(R)*-isomers for the cyclopentenyl RHS. Detailed synthetic procedures are described in the Experimental Section and Supporting Information. N.D.: not determined. [b]PFI = Chrom $logD_{pH7.4}$ + # Ar, and Chrom $logD_{pH7.4}$ was measured.[30] [c]CXCR2 Tango assay pIC_{50} value is the average of at least two measurements. [d]Solubility was measured after 4 h incubation. [e]Detailed assay protocol to measure efflux ratio is described in the Experimental Section. [f]Permeability ratio. [g]Using predicted $logD_{pH7.4}$ value from ACD software, version 11.0.

Table 4. CNS Penetration Profile of CXCR2 Antagonist **40**–**42** and **50**–**52**[a]

Cmpd	Blood $DNAUC_{0-7h}$ (ng·h/mL)/(mg/kg)	Brain $DNAUC_{0-7h}$ (ng·h/g)/(mg/kg)	K_p[b]	$F_{u,br}$[c]	$F_{u,bl}$[d]	$K_{p,uu}$[e]
40	614	97	0.16	3.4%	1.1%	0.48
41	535	107	0.20	2.1%	0.70%	0.59
42	4331	243	0.06	5.1%	0.65%	N.D.
50	2580	161	0.06	13.7%	5.0%	N.D.
51	11721	296	0.03	11.4%	0.65%	N.D.
52	2575	73	0.03	11.6%	3.4%	N.D.

[a]CNS penetration was measured using in *vivo* rat SOA model. Detailed protocol is described the Experimental Section. N.D.: not determined. [b]K_p = brain $DNAUC_{0-7h}$/blood $DNAUC_{0-7h}$. [c]Free unbound fraction measured in rat brain. [d]Free unbound fraction measured in rat blood. [e]$K_{p,uu} = K_p \times Fu_{br}/Fu_{bl}$.

Table 5. Selected SAR of Oxygen-containing R^1 Substituent Exploration[a]

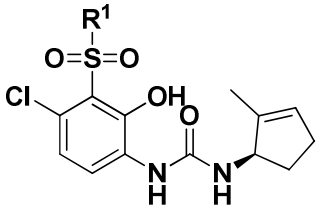

54–**71**

Cmpd	R^1	MW/ PFI[b]	CXCR2 Tango pIC_{50}[c]	FaSSIF sol. (μg/mL)[d]	Pgp/BCRP efflux ratio[e]	Perm. (nm/s)	HWB CD11b pIC_{50}

54	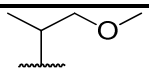	403/5.7	8.9	72.0	3.2	282	6.4
55	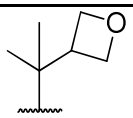	429/6.3[g]	9.6	7.0	3.2	296	N.D.
56	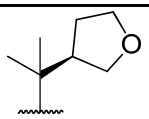	443/6.8	8.8	25.2	2.2	331	6.5
57	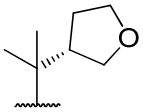	443/6.8	8.9	24.6	4.5[f]	127	N.D.
58	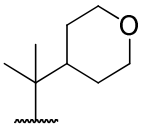	457/7.2	9.3	1.4	3.9	303	6.4
59	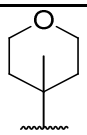	429/6.4	9.3	6.1	3.4	532	6.7
60	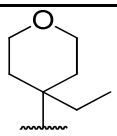	443/6.9	9.5	16.0	3.2	324	6.4
61	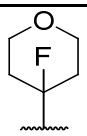	433/5.3	9.7	3.3	6.2	323	7.2
62	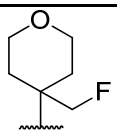	447/5.6	8.9	14.9	18.7	218	6.6
63	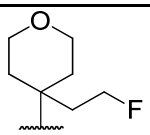	461/5.9	7.5	26.7	10.8	337	N.D.
64	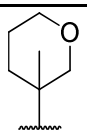	429/6.7	8.7	4.1	3.4	267	6.7

65	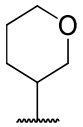	415/5.4	8.8	13.7	9.6	263	6.6
66	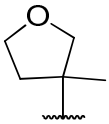	415/5.7	8.9	33.2	3.8	318	6.9
67	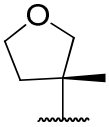	415/5.8	9.0	20.5	2.4[f]	252	6.8
68	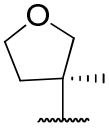	415/5.8	9.0	21.0	2.0	254	7.4
69	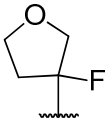	419/4.3	9.1	39.0	7.0	281	N.D.
70	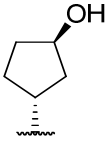	415/4.4	9.6	15.1	26.8	72	N.D.
71	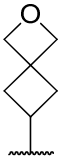	427/4.9	9.0	126.6	25.5	124	N.D.

[a]All compounds were prepared and tested as known single *(R)*-isomers for the cyclopentenyl RHS. Detailed synthetic procedures are described in the Experimental Section and Supporting Information. N.D.: not determined. [b]PFI = Chrom $logD_{pH7.4}$ + # Ar, and Chrom $logD_{pH7.4}$ was measured.[30] [c]CXCR2 Tango assay pIC_{50} value is the average of at least two measurements. [d]Solubility was measured after 4 h incubation. [e]Detailed assay protocol to measure efflux ratio (ER) is described in the Experimental Section. [f]Permeability ratio. [g]Using predicted $logD_{pH7.4}$ value from ACD software, version 11.0.

Table 6. CNS Penetration Profile of CXCR2 Antagonists **56**, **67**, and **68**.[a]

Cmpd	Blood $DNAUC_{0\text{-}7h}$	Brain $DNAUC_{0\text{-}7h}$	K_p[b]	$F_{u,br}$[c]	$F_{u,bl}$[d]	$K_{p,uu}$[e]

	(ng·h/mL)/(mg/kg)	(ng·h/g)/(mg/kg)				
56	63.8	13.4	0.21	3.3%	1.6%	0.42
67	788	60.5	0.08	10.6%	3.6%	0.23
68	651	87.7	0.14	12.3%	2.7%	0.63

[a]CNS penetration was measured using in *vivo* rat SOA model. Detailed protocol is described the Experimental Section. [b]K_p = brain $DNAUC_{0\text{-}7h}$/blood $DNAUC_{0\text{-}7h}$. [c]Free unbound fraction measured in rat brain. [d]Free unbound fraction measured in rat blood. [e]$K_{p,uu} = K_p \times Fu_{br}/Fu_{bl}$.

Table 7. DMPK Profile of Lead Compounds **40** and **68**[a]

	40	**68**	
	Rat	Rat	Dog
In vivo PK			
IV dose (mg/kg)	1.01	0.98	0.85
Cl_b (mL/min/kg)	15.7	9.1	5.6
V_{ss} (L/Kg)	2.2	2.1	0.88
$T_{1/2}$ (h)	2.5	4.3	3.6
$DNAUC_{0\sim\infty}$ (ng·h/mL)/(mg/kg)	1071	1829	2996
oral dose (mg/kg)	2.38	2.41	1.29
T_{max} (h)	2.5	1.0	1.1
C_{max} (ng/mL)	292	452	728
$DNAUC_{0\sim\infty}$ (ng·h/mL)/(mg/kg)	961	860	2298
F (%)	88	47	76

Table 8. Metabolic Stability of Lead Compound **68** in Human, Rat, and Dog Hepatocytes

Metabolic stability	**68**
Human Cl_{int} (mL/min/g)	0.79
Rat Cl_{int} (mL/min/g)	7.7
Dog Cl_{int} (mL/min/g)	1.8

Table 9. Chemokine Selectivity Profile of Lead Compound **68**[a]

Assay target	Agonism EC_{50} (μM)	Antagonism IC_{50} (μM)

CCR10	>10	>10
CCR2	>10	>10
CCR3	>10	>10
CCR4	>10	>10
CCR5	>10	>10
CCR6	>10	>10
CCR7	>10	>10
CCR8	>10	>10
CCR9	>10	>10
CMKLR1	>10	>10
CXC3R1	>10	>10
CXCR1	>10	3.8
CXCR2	>10	0.0052
CXCR3	>10	>10
CXCR4	>10	>10
CXCR5	>10	>10
CXCR6	>10	>10
CXCR7	>10	>10

TABLE OF CONTENTS GRAPHIC.

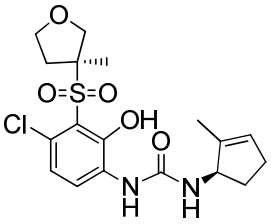

68

CXCR2 Tango IC_{50} = 1 nM
HWB IC_{50} = 0.04 uM
Fu_{br} (r) = 12.3%; $K_{p,uu}$ (r) = 0.63
F% (r) = 47%; F% (d) = 76%